Biol Cybern (2010) 103:365–386
DOI 10.1007/s00422-010-0405-7

ORIGINAL PAPER

Biological Cybernetics

Emergence of network structure due to spike-timing-dependent plasticity in recurrent neuronal networks V: self-organization schemes and weight dependence

Matthieu Gilson · Anthony N. Burkitt · David B. Grayden · Doreen A. Thomas · J. Leo van Hemmen

Received: 25 December 2009 / Accepted: 23 August 2010 / Published online: 29 September 2010

Abstract Spike-timing-dependent plasticity (STDP) determines the evolution of the synaptic weights according to their pre- and post-synaptic activity, which in turn changes the neuronal activity on a (much) slower time scale. This paper examines the effect of STDP in a recurrently connected network stimulated by external pools of input spike trains, where both input and recurrent synapses are plastic. Our previously developed theoretical framework is extended to incorporate weight-dependent STDP and dendritic delays. The weight dynamics is determined by an interplay between the neuronal activation mechanisms, the input spike-time correlations, and the learning parameters. For the case of two external input pools, the resulting learning scheme can exhibit a symmetry breaking of the input connections such that two neuronal groups emerge, each specialized to one input pool only. In addition, we show how the recurrent connections within each neuronal group can be strengthened by STDP at the expense of those between the two groups. This neuronal self-organization can be seen as a basic dynamical ingredient for the emergence of neuronal maps induced by activity-dependent plasticity.

M. Gilson (✉) · A. N. Burkitt · D. B. Grayden · D. A. Thomas
Department of Electrical and Electronic Engineering,
University of Melbourne, Melbourne, VIC 3010, Australia
e-mail: gilsonm@unimelb.edu.au

M. Gilson · A. N. Burkitt · D. B. Grayden
The Bionic Ear Institute, 384-388 Albert St, East Melbourne,
VIC 3002, Australia

M. Gilson · A. N. Burkitt · D. B. Grayden · D. A. Thomas
NICTA, Victoria Research Lab, University of Melbourne,
Melbourne, VIC 3010, Australia

J. L. van Hemmen
Physik Department (T35) and BCCN-Munich, Technische
Universität München, 85747 Garching bei München, Germany

Keywords Learning · Weight-dependent STDP · Recurrent neuronal network · Spike-time correlation · Self-organization

1 Introduction

Object recognition in the visual pathway and sound localization in the auditory pathway are examples of sophisticated computational tasks performed thanks to elaborate neuronal circuitry in the brain. This organization is not mature yet at birth, but is rather acquired during the first years of a mammal's life. In this work, we get inspiration from neuronal maps, namely networks where neighboring neurons are sensitive to external stimuli that possess some similarity (deCharms and Zador 2000). As an example, the primary visual cortex is organized in areas responsive to different features of visual perception, such as orientation fields and ocular dominance (Hubel and Wiesel 1962). The development of such synaptic connectivity relies on both neurogenerative mechanisms, such as the creation of synapses and the growth of axons using chemical markers, and activity-dependent plasticity, meaning the strengthening or weakening of existing synapses due to the neuronal spiking activity (Katz and Crowley 2002; Hensch 2005; Hirsch and Martinez 2006). Several rounds of organization first shape and then refined the synaptic connectivity. In particular, neurons exhibit different types of electrical activity throughout the maturation process (Zhang and Poo 2001). Schematically speaking, initial phases involve spontaneous neuronal activity alone, whereas later stages fine tune the circuitry using also responses to external stimuli conveyed by upstream sensory pathways (e.g., thalamic inputs for sensory cortices).

The present paper examines how activity-dependent plasticity, which modifies existing synaptic connections, can

generate network structure among recurrently connected neurons stimulated by external (input) spike trains. Basically, the latter can account for either spontaneous or experience-driven activity that excites a given local neuronal network. Many theoretical studies have examined suitable conditions on the learning rules, pre-existing connectivity topology, and/or input structure that allow the emergence of physiologically realistic cortical organization (Malsburg 1973; Kohonen 1982; Swindale 1996; Elliott and Shadbolt 1999; Goodhill 2007). By meaningful network structure, we mean synaptic connectivity that reflects and/or is adapted to process the input functional pathways. This paper considers an idealized network where both input and recurrent connections are simultaneously plastic and initially unorganized. We do not discriminate between input and recurrent synapses, although the theoretical framework is fitted to incorporate such a refinement. In this way, we focus on the relationship between learning dynamics and the input configuration.

Numerous experimental studies have produced evidence for the importance of the fine spike-timing (at the scale of milliseconds) in synaptic plasticity occurring in various brain areas such as hippocampus and neocortex (Markram et al. 1997; Bell et al. 1997; Magee and Johnston 1997; Bi and Poo 1998; Debanne et al. 1998; Egger et al. 1999; Feldman 2000; Bi and Poo 2001; Boettiger and Doupe 2001; Sjöström et al. 2001; Froemke and Dan 2002; Tzounopoulos et al. 2004). In glutamatergic (excitatory) synapses, such spike-timing-dependent plasticity (STDP) relies on a complex relationship involving, in particular, NMDA receptors and the local concentration in Ca^{2+} ions (Markram et al. 1997; Debanne et al. 1998; Bi and Poo 1998; Sjöström et al. 2001). The timing of the pre- and post-synaptic activity is captured in the kinetics of Ca^{2+} (Magee and Johnston 1997; Sabatini et al. 2002; Rubin et al. 2005). Moreover, experimental studies have shown evidence that the weight change depends upon the current value of the synaptic strength (Bi and Poo 1998; Wang et al. 2005). At high spiking rates, Sjöström et al. (2001) showed that not all pairs of pre- and post-synaptic spikes contribute to STDP. For reviews, see Dan and Poo (2006) and Caporale and Dan (2008).

Within the context of neuronal networks with recurrent (feedback) connections, it is not yet clear how STDP can tune the spiking activity. In order to investigate its functional effects, we use a phenomenological model that abstracts some key features observed in physiology (Morrison et al. 2008). We limit our study to plasticity induced by single spikes and pairs of spikes, where all pairs contribute to STDP. In this way, we focus on the relationship between the pairwise spike-time correlation and the weight dynamics; higher-order interactions are left to subsequent studies. This choice has limitations compared to more elaborate models that include triplets of spikes in their analysis (Sjöström et al. 2001; Pfister and Gerstner 2006; Appleby and Elliott 2006) or spike-pair restrictions (Sjöström et al. 2001; Izhikevich and Desai 2003; Burkitt et al. 2004). We also incorporate weight-dependent (non-additive) STDP (Markram et al. 1997; Bi and Poo 1998, 2001; Gütig et al. 2003; Meffin et al. 2006; Morrison et al. 2007) in our previously developed framework (Gilson et al. 2009a,d). For illustration purpose, we use a model proposed by Gütig et al. (2003) that exhibits two different types of behaviors when varying a parameter that determines the strength of the weight dependence: for a neuron stimulated by two identical input pools, the weight distribution can become either unimodal or bimodal. The transition (bifurcation) between these two classes of behavior for STDP depends upon the input correlation level. An interesting scenario is one in which symmetry breaking (synonymous with neuronal specialization) occurs for sufficiently strong input correlation (Gütig et al. 2003; Meffin et al. 2006), but the initial weight distribution is preserved for uncorrelated inputs.

Even though STDP can be used in rate-based mode, we focus here on learning dynamics that are specific to spike-based plasticity and examine differences between these two classes of learning rules. First, STDP can capture spike-time information at the scale of milliseconds, which can explain how barn owls can tune their hearing system (Gerstner et al. 1996). Second, and as a consequence, STDP can generate learning dynamics involving simultaneously stability and competition (Kempter et al. 1999). In this scheme, competition mainly relies on spike-time correlations, whereas stability relates to firing rates. Such "double" dynamics has been the subject of many studies for rate-based plasticity rules (Bienenstock et al. 1982; Elliott 2003; Miller and Mackay 1994; Miller 1996; Goodhill and Barrow 1994) to obtain effective input selectivity. We will examine how weight specialization can arise (and benefit) from dynamics intrinsic to STDP in a recurrently connected network.

The present paper focuses on neuronal specialization induced by STDP in a recurrent network stimulated by pools of external inputs that have narrow spike-time correlations (Kempter et al. 1999; Song and Abbott 2001; Gütig et al. 2003; Meffin et al. 2006). Both input and recurrent synaptic connections are plastic, as illustrated in Fig. 1. We constrain our study to excitatory synapses and inhibition is not considered in detail (identical for all neurons in the network). The relationship between STDP and spike-time information is presented in Sect. 2, together with learning equations that describe the evolution of the synaptic weights. In a sense, spike-based plasticity extends "classical" Hebbian rate-based models with an additional term in the learning equations, which has profound implications in the resulting dynamics. The learning framework (Burkitt et al. 2007; Gilson et al. 2009a,d) is briefly recapitulated in Sect. 3 and the constraints imposed by the recurrent connectivity upon the time-averaged firing rates and pairwise spike-time correlations are

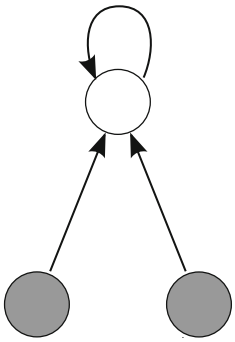

Fig. 1 Schematic diagram representing a recurrently connected network stimulated by two pools of inputs where both input and recurrent connections are plastic

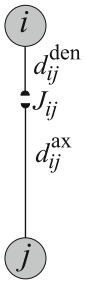

Fig. 2 Schematic representation of a synapse from the source neuron j to the target neuron i. The synapse is determined by the weight J_{ij}, dendritic delay d_{ij}^{den}, and axonal delay d_{ij}^{ax}

described. This framework is complementary to other analytical work that studies the effect of STDP in the presence of oscillatory activity (Câteau et al. 2008). It can be applied to any network topology and input structure; its main limitation concerns the Poisson neuron model used in the derivation, which approximates satisfactorily only some regimes of real neurons, but allows tractable calculations. We adapt analytical tools previously developed for additive STDP (Gilson et al. 2009a,b,c,d) to the present case of non-additive STDP. Our results also aim to shed light on previous studies on neuronal specialization that mainly used numerical simulation for various connectivity topologies (Choe and Miikkulainen 1998; Song et al. 2000; Song and Abbott 2001; Wenisch et al. 2005; Morrison et al. 2007). In this way, we bridge the gap between the neuronal and the network levels: how a local plasticity rule relying on spike-time correlations can generate rich network structure. The study of the functional implications of STDP in recurrently connected networks highlights the roles of the main players: neuronal and synaptic mechanisms, structure of the stimulating inputs, network connectivity, and learning parameters.

2 Spike-based learning and spiking activity

In this section, we adapt the model of additive STDP that we used previously (Gilson et al. 2009a,b,c,d) in order to incorporate the dependence of the learning rule upon the current value of the weight. In addition, we consider the effect of dendritic and axonal delays.

2.1 Pairwise weight-dependent STDP

For two neurons i and j connected by a synapse $j \to i$ as illustrated in Fig. 2, a pre-synaptic spike fired at time t_j will affect the synapse at time $t_{\text{in}} = t_j + d_{ij}^{\text{ax}}$; likewise, the effect of a post-synaptic spike at time t_i will occur at the starting time $t_{\text{out}} = t_i + d_{ij}^{\text{den}}$. We consider a weight-dependent version of STDP to describe the change in the weight J_{ij} due to single spikes and pairs of spikes (van Rossum et al. 2000; Bi and Poo 2001; Gütig et al. 2003; Morrison et al. 2007). A sole pair of pre- and post-synaptic spikes fired at respective times t_j and t_i induces a weight change δJ_{ij} determined by the following contributions:

$$\delta J_{ij} = \eta \begin{cases} w^{\text{in}} & \text{at time } t_{\text{in}}, \\ w^{\text{out}} & \text{at time } t_{\text{out}}, \\ f_+(J_{ij})\, W_+(t_{\text{in}} - t_{\text{out}}) & \text{if } t_{\text{in}} < t_{\text{out}}, \\ -f_-(J_{ij})\, W_-(t_{\text{in}} - t_{\text{out}}) & \text{if } t_{\text{in}} > t_{\text{out}}, \end{cases}$$

where $t_{\text{in}} = t_j + d_{ij}^{\text{ax}}$ and $t_{\text{out}} = t_i + d_{ij}^{\text{den}}$. The rate-based contributions w^{in} and w^{out} occur once for each pre- and post-synaptic spike, respectively (Kempter et al. 1999; Burkitt et al. 2007). They have been used previously with additive STDP to obtain stability (as will be described later); we will discuss their implications in the learning dynamics. The STDP learning window function W_- (resp., W_+) describes the depression (potentiation) of the weight J_{ij} depending on the difference between the spike times $t^{\text{in}} - t^{\text{out}}$ when it is positive (negative), as illustrated in Fig. 3a; this contribution is rescaled by f_- (resp., f_+) as a function of the value of the weight J. The functions f_-, f_+, W_-, and W_+ are non-negative, which corresponds to Hebbian learning. All these contributions are scaled by a learning parameter, typically chosen to be very small, $\eta \ll 1$, to model learning processes that occur very slowly compared to the other neuronal and synaptic mechanisms.

The following analysis will be carried out for arbitrary functions $f_\pm$. To illustrate the effect of non-additive STDP, we use the same functions f_+ and f_- as Gütig et al. (2003),

$$f_+(J_{ij}) = \left(1 - \frac{J_{ij}}{J_{\max}}\right)^\gamma \quad \text{and} \quad f_-(J_{ij}) = \left(\frac{J_{ij}}{J_{\max}}\right)^\gamma, \qquad (1)$$

where the parameter $0 \le \gamma \le 1$ scales between additive STDP ($\gamma = 0$) and multiplicative STDP ($\gamma = 1$) for both functions; $J_{\max}$ is the upper "soft" bound, while the lower "soft" bound is zero, as illustrated in Fig. 3b. This choice is motivated by investigating the effect of the weight dependence "strength": larger values for γ lead to narrower asymptotic weight distribution clustered around their mean, whereas smaller values induce stronger competition that can split the the distribution of incoming weights.

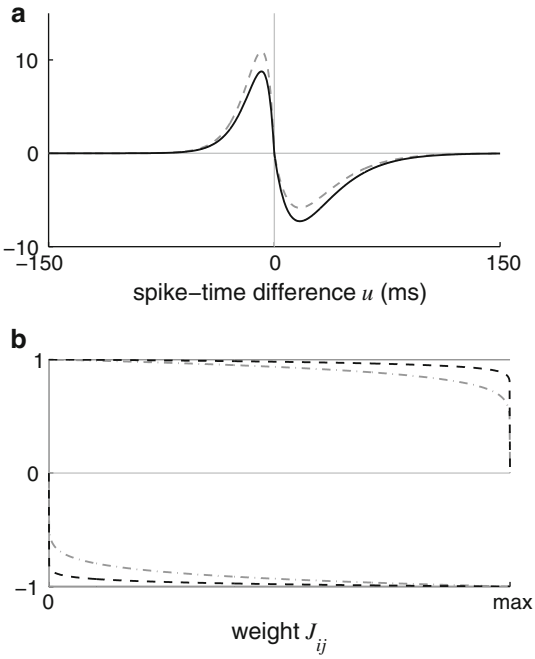

Fig. 3 Example of STDP window function. **a** The dependence upon the spike-time difference u is captured by one alpha function W_+ for potentiation (*left side*) with time constant 8.5 ms and one alpha function W_- for depression (*right side*) with 17 ms. The weight dependence leads to more depression and less potentiation for a strong synapse ($J_{ij} = 0.9 J_{\max}$, *black solid line*) than a weak synapse ($J_{ij} = 0.1 J_{\max}$, *gray dashed line*); the curve corresponds to $\gamma = 0.1$ in (1). **b** Plots of the scaling functions f_+ and $-f_-$ defined in (1) that determine the weight dependence: almost-additive STDP with $\gamma = 0.03$ (*dashed line*) and medium weight dependence with $\gamma = 0.1$ (*dashed-dotted line*). The *gray solid lines* at ± 1 correspond to additive STDP. See Appendix A for parameter details

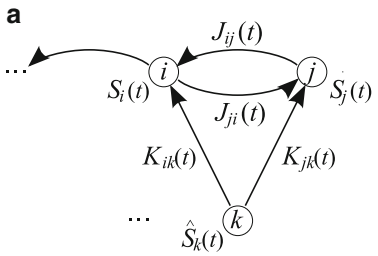

b

	input-to-input	neuron-to-input	neuron-to-neuron
firing rates	$\hat{\nu}_k(t)$		$\nu_i(t)$
covar coeff	$\hat{C}_{kl}(t,u)$	$F_{ik}(t,u)$	$C_{ij}(t,u)$
weights		$K_{ik}(t)$	$J_{ij}(t)$
dendritic delays		$\hat{d}^{\text{den}}_{ik}$	d^{den}_{ij}
axonal delays		$\hat{d}^{\text{ax}}_{ik}$	d^{ax}_{ij}

Fig. 4 Presentation of the network and notation. **a** Schematic representation of the network: two of the N neurons (*top circles*, indexed by $1 \le i \le N$) receive one of the M external input spike trains (*bottom circle*, $1 \le k \le M$). Both the input and recurrent connections (*thick arrows*) have plastic weights, K_{ik} and J_{ij}, respectively. The neuron and input spike trains are denoted by S_i and $\hat{S}_k$, respectively. **b** The table shows the variables that describe the neuronal and input spiking activity (time-averaged firing rates $\hat{\boldsymbol{\nu}}$ and $\boldsymbol{\nu}$; time-averaged covariances $\hat{C}$, F and C), and those related to the synaptic connections $k \to i$ and $j \to i$ (weights K and J; delays $\hat{d}$ and d)

2.2 Capturing mean effect of slow learning: separation of time scales in neuronal spiking activity

We consider the general situation of a network of N recurrently connected neurons stimulated by M external input spike trains, as illustrated in Fig. 4a. In a similar manner to Kempter et al. (1999) and Gilson et al. (2009a,d), we use the adiabatic assumption of slow learning compared to the neuronal spiking dynamics to evaluate the change in the synaptic weight (van Hemmen 2001). When the input spike trains involve probabilistic variability in their spike times and/or the neuronal spiking mechanisms are stochastic (this is the case for the Poisson neuron used throughout this paper), the evolution of the weights is also stochastic and can be studied through their expectation value (or drift) and higher moments of the weight dynamics (Kempter et al. 1999; Gütig et al. 2003; Meffin et al. 2006). Details of the following results are provided by Gilson et al. (2009a,d, Sect. 2.3 in both articles), the extension here lies in considering the two sides of STDP for potentiation and depression separately, because we use weight-dependent STDP.

We obtain a differential equation to describe the evolution of the drift of the input weight K_{ik}

$$\begin{aligned}\dot{K}_{ik} \simeq \eta \Big\{ & w^{\text{in}}\, \hat{\nu}_k \;+\; w^{\text{out}}\, \nu_i \\ & + \big[f_+(K_{ik})\, \widetilde{W}_+ \;-\; f_-(K_{ik})\, \widetilde{W}_- \big]\, \hat{\nu}_k\, \nu_i \\ & + f_+(K_{ik})\, F^{W_+}_{ik} \;-\; f_-(K_{ik})\, F^{W_-}_{ik} \Big\}, \end{aligned} \tag{2}$$

where

$$\widetilde{W}_\pm \;:=\; \int W_\pm(u)\, \mathrm{d}u. \tag{3}$$

The weight change in (2) is expressed in terms of the time-averaged firing rate (over a period T) for neuron i

$$\nu_i(t) \;:=\; \frac{1}{T} \int_{t-T}^{t} \big\langle S_i(t') \big\rangle\, \mathrm{d}t', \tag{4}$$

where $\langle S_i(t) \rangle$ is the instantaneous firing rate, the time-averaged firing rate $\hat{\nu}_k(t)$ for input k, and their time-averaged spike-time covariance

$$F_{ik}(t,u) := \frac{1}{T}\int_{t-T}^{t} \left\langle S_i(t')\,\hat{S}_k(t'+u)\right\rangle \mathrm{d}t' - \frac{1}{T}\int_{t-T}^{t} \left\langle S_i(t')\right\rangle \left\langle \hat{S}_k(t'+u)\right\rangle \mathrm{d}t',$$

$$F_{ik}^{W_\pm}(t) := \int_{-\infty}^{+\infty} W_\pm\left(u+\hat{d}_{ik}^{\mathrm{ax}}-\hat{d}_{ik}^{\mathrm{den}}\right) F_{ik}(t,u)\,\mathrm{d}u. \qquad (5)$$

A similar equation is derived for the drift of the recurrent weight J_{ij} (Gilson et al. 2009d, Sect. 2.3.2)

$$\dot{J}_{ij} \simeq \eta\left\{w^{\mathrm{in}}\,\nu_j + w^{\mathrm{out}}\,\nu_i + \left[f_+(J_{ij})\,\widetilde{W}_+ - f_-(J_{ij})\widetilde{W}_-\right]\nu_j\,\nu_i + f_+(J_{ij})\,C_{ij}^{W_+} - f_-(J_{ij})\,C_{ij}^{W_-}\right\}, \qquad (6)$$

with the time-averaged spike-time covariance between neurons i and j

$$C_{ij}(t) := \frac{1}{T}\int_{t-T}^{t} \left\langle S_i(t')\,S_j(t'+u)\right\rangle \mathrm{d}t' - \frac{1}{T}\int_{t-T}^{t} \left\langle S_i(t')\right\rangle \left\langle S_j(t'+u)\right\rangle \mathrm{d}t',$$

$$C_{ij}^{W_\pm}(t) := \int_{-\infty}^{+\infty} W_\pm\left(u+d_{ij}^{\mathrm{ax}}-d_{ij}^{\mathrm{den}}\right) C_{ij}(t,u)\,\mathrm{d}u. \qquad (7)$$

The effect of our model of STDP is thus completely described by the network variables summarized in Fig. 4b.

For the sake of simplicity, we will use matrix notation in the remainder of the text: vectors (in bold fonts) $\boldsymbol{\nu}$ and $\hat{\boldsymbol{\nu}}$ and matrices C, F, J, and K.

2.3 Relationship to rate-based learning rules

The averaging period T in (4), (5), and (7) can be chosen as an intermediate time scale between the "fast" neuronal and synaptic mechanisms and the "slow" learning process (Kempter et al. 1999; Burkitt et al. 2007; Gilson et al. 2009a). This implies a low pass filtering of the spike trains in the information contained in the time-averaged firing rates ($\boldsymbol{\nu}$ and $\hat{\boldsymbol{\nu}}$). Spike-time information at a short-time scale (order of milliseconds) is, however, present in C and F: these variables describe, for each input/neuron or neuron/neuron pair, the mutual fast covariations of their firing probabilities. These cross-correlograms are convolved with the learning window functions $W_\pm$ to obtain the coefficients $C^{W_\pm}$ and $F^{W_\pm}$ that appear in (2) and (6). Therefore, the functions $W_\pm$ determine the time scale below which variations of the firing probabilities are considered spike effects. With our choice of parameters (Appendix A), the corresponding range lies below 100 ms (i.e., above 10 Hz).

Rate-based models only involve $\boldsymbol{\nu}$ and $\hat{\boldsymbol{\nu}}$ and, thus, ignore the spike-time correlations. In this sense, STDP extends rate-based learning with the additional terms involving F and C. The analysis of the learning dynamics for additive STDP (Gilson et al. 2009a,c, Sect. 3) has shown how the time-averaged firing rates can lead to the stabilization of the mean incoming weight for each neuron. For a broad range of learning parameters, stable and non-saturated neuronal firing rates $\boldsymbol{\nu}$ can be obtained via (anti-Hebbian) rate-based dynamics. When spike-time correlations are present, the weights become structured, driven by terms in the dynamical equations depending upon the covariance coefficients F and C. These spike-based contributions induce a diverging behavior in some subspace where the weight matrices evolve and lead to functional specialization of the neurons. Provided the input firing rates are not too unbalanced, the emerging specialization is rather determined by spike-time correlations. This mixture of a partial equilibrium and diverging behavior ensures a robust weight specialization (Kempter et al. 1999; Gilson et al. 2009a,d). For some choices of parameters, weight-dependent STDP, which is non-linear with respect to the weight strength, was shown to exhibit a similar behavior for single neurons (Gütig et al. 2003; Meffin et al. 2006). Relying on rate correlations (slower timescale), rate-based learning rules can produce similarly rich dynamics when equipped with appropriate non-linearity (Bienenstock et al. 1982; Goodhill and Barrow 1994; Elliott 2003). The remainder of this paper examines how spike effects can lead to network structure when using weight-dependent STDP (Sect. 2.1).

2.4 Input spike-time correlation structure

Throughout this series of papers (Gilson et al. 2009a,b,c,d), the input structure is modeled using a "simple" configuration: mixed Poisson processes that have narrow spike-time correlations, as illustrated in Fig. 5. To illustrate our analysis, we will consider two pools of external inputs that have within-pool correlations, but no between-pool correlations. Such a configuration has been used to model ocular pathways (Song and Abbott 2001): spike trains coming from the same eye have correlated activity at a short time scale, whereas those from different eyes are uncorrelated. A connection to physiology can be made with, for example, spontaneous retinal waves of spiking activity that propagate toward the brain via the optic nerves during the development of young mammals (Wong 1999; Butts et al. 2007).

In the present paper, we use the same configuration, where the input spiking information is contained in the firing rates and spike-time correlations. For inputs k and l, we define

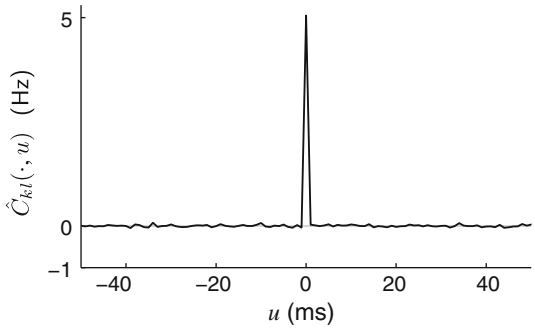

Fig. 5 Cross-correlogram between two inputs from the same correlated pool. The simulated curve (*solid line*) that corresponds to (8) averaged over 1000 s agrees with the prediction in (9) with $\hat{\nu}_0 = 20$ Hz and $\hat{c} = 0.25$; the histogram bin is 1 ms

$$\hat{C}_{kl}(t,u) := \frac{1}{T}\int_{t-T}^{t} \left\langle \hat{S}_k(t')\,\hat{S}_l(t'+u)\right\rangle \mathrm{d}t', \\ -\frac{1}{T}\int_{t-T}^{t} \left\langle \hat{S}_k(t')\right\rangle \left\langle \hat{S}_l(t'+u)\right\rangle \mathrm{d}t'. \tag{8}$$

The firing rates of inputs within a pool are all identical. Positive within-pool correlation is generated so that, for any input, a portion of its spikes occur at the same time as some other spikes within its pool, while the remaining spikes occur at independent times (Gütig et al. 2003; Meffin et al. 2006). In this way, we obtain input spike trains $\hat{S}_k(t)$ with "instantaneous" firing rates $\langle \hat{S}_k(t)\rangle = \hat{\nu}_0$ and pairwise covariances $\hat{C}_{kl}(t,u)$ defined in (8) that satisfy

$$\hat{C}_{kl}(t,u) \simeq \hat{c}\,\hat{\nu}_0\,\delta(u), \tag{9}$$

where $0 \le \hat{c} \le 0.25$ is the correlation strength (chosen to be small) and δ is the Dirac delta-function. Hence, we refer to this configuration as "delta-correlated" inputs, cf. the peak at $\hat{c}\,\hat{\nu}_0 = 5$ Hz for $\hat{\nu}_0 = 20$ Hz and $\hat{c} = 0.25$ in Fig. 5. See Gilson et al. (2009a, Sect. 2.3.7) for more detail.

The learning equations (2) and (6) show that the weight change induced by our model of STDP is expressed in terms of the neuronal firing rates $\boldsymbol{\nu}$, the neuron-to-input and neuron-to-neuron correlation structures F and C, as well as the weight scaling functions $f_\pm$. In the same way as in our previous analysis using additive STDP (Gilson et al. 2009a,d), it is necessary to express these spike-time correlation structures in terms of the input-to-input correlation structure $\hat{C}$ in order to evaluate the weight evolution.

3 Modeling neuronal activity to evaluate learning dynamics

The previous section did not consider the neuronal model; the learning equations are valid provided the spike trains, as stochastic point processes, are second-order stationary. This relates to the ergodicity of the network spiking activity and means that the firing rates and spike-time covariances used in the previous section are well defined. The latter applies, for example, to a network of Poisson neurons, or integrate-and-fire neurons as they are renewal processes (Burkitt 2006).

Now we use the Poisson neuron model in order to express the variables describing the neuronal activity $\boldsymbol{\nu}$, F and C in terms of those for the external inputs $\hat{\boldsymbol{\nu}}$ and $\hat{C}$. The following equations are strictly valid for a network with fixed weights (Hawkes 1971; Massoulie 1998), but they provide a good approximation in the case of slow learning when the external inputs have fixed firing rates and covariances (Kempter et al. 1999; Gilson et al. 2009a,d).

3.1 Poisson neuron model

The spiking mechanism of a given neuron i is approximated by an inhomogeneous Poisson process driven by an intensity function $\rho_i(t)$ in order to generate an output spike-time series $S_i(t)$ (Kempter et al. 1999). The rate function $\rho_i(t)$ relates to the soma potential and it evolves over time according to the excitation received from other neurons $j \neq i$:

$$\rho_i(t) = \nu_0 + \sum_{j\neq i}\left[J_{ij}(t)\sum_n \epsilon\left(t - t_{j,n} - d_{ij}^{\mathrm{den}} - d_{ij}^{\mathrm{ax}}\right)\right] \\ + \sum_k \left[K_{ik}(t)\sum_n \epsilon\left(t - \hat{t}_{k,n} - \hat{d}_{ik}^{\mathrm{den}} - \hat{d}_{ik}^{\mathrm{ax}}\right)\right]. \tag{10}$$

The constant ν_0 is the spontaneous firing rate (identical for all neurons), which accounts for other pre-synaptic connections that are not considered in detail. Each pre-synaptic spike induces a variation of $\rho_i(t)$ taken care of by the post-synaptic potential (PSP), which is determined by the synaptic weights J_{ij}, the post-synaptic response kernel ϵ, and the delays d_{ij}. The kernel function ϵ models the PSP due to the current injected into the post-synaptic neuron as a consequence of one single pre-synaptic spike; $\epsilon(t)$ is normalized to one: $\int \epsilon(t)\mathrm{d}t = 1$; and in order to preserve causality, we have $\epsilon(t) = 0$ for $t < 0$. The delays account for the axonal transmission, the neurotransmitter diffusion, and the dendritic transmission such that the nth spike fired by neuron j at time $t_{j,n}$ begins to affect the soma potential of neuron i at time $t_{j,n} + d_{ij}^{\mathrm{den}} + d_{ij}^{\mathrm{ax}}$. Self-connections are forbidden and, for simplicity, we assume the same kernel function ϵ for both input and recurrent synapses, but this is not crucial in the subsequent study. However, further analysis is required when input and recurrent connections have significantly distinct properties (e.g., for thalamocortical and intracortical synapses), but this is out of the scope of the present paper. Likewise, we will use similar numbers of inputs and neurons M and N in numerical simulation, but the analysis is carried out for arbitrary values; we do not focus on weight dynamics

effects that have been specifically observed in large networks by Morrison et al. (2007), though.

A Poisson neuron exhibits an irregular output spike train, similar to some physiological observations in cortex (Shadlen and Newsome 1998). Its mathematical simplicity has proven to be useful to obtain analytical results about the weight dynamics that can be qualitatively transposed to the case of integrate-and-fire neurons (Kempter et al. 1999; Gütig et al. 2003). However, we keep in mind that, for example, the spiking activity of type-II neurons that exhibit strong synchronization or integrate-and-fire with hyperpolarized sub-threshold equilibrium voltage may only be poorly approximated by this model.

3.2 Consistency equations for neuronal activity related to network constraints

The following consistency equations describe the effect of the synaptic filtering together with the constraint of the input and recurrent connectivity upon the variables $\boldsymbol{\nu}$, F, and C. In addition to the assumption of second-order stationarity mentioned above, each set of axonal and dendritic delays are considered to exhibit narrow distributions, both for the input and recurrent connections: e.g., $d_{ij}^{\mathrm{den}} \simeq d^{\mathrm{den}}$ for all connections $j \to i$. In order to obtain tractable equations that give at the same time a good approximation, we further require short durations for the recurrent delays $d_{ij}^{\mathrm{den}} + d_{ij}^{\mathrm{ax}}$ and the PSP kernel ϵ compared to the time scale of $W_{\pm}$. Further analysis is necessary to examine in more detail the effect of longer time constants for the recurrent delays and ϵ, for example, with similar time constants to $W_{\pm}$, which is relevant in some neuronal systems (Pfister et al. 2006a); this is beyond the scope of the present paper and left for subsequent study. Details of the derivation are provided by Gilson et al. (2009a,d, Appendices), which leads to the following matrix equations:

$$\boldsymbol{\nu} = (\mathbb{1}_N - J)^{-1} \left(\nu_0\, \mathbf{e} + K\, \hat{\boldsymbol{\nu}}\right), \tag{11a}$$

$$\int F(\cdot,u)\,\Psi(u)\,\mathrm{d}u \simeq (\mathbb{1}_N - J)^{-1}\, K \int \hat{C}(\cdot,u)\,(\Psi * \epsilon)\,(u - \hat{d}^{\mathrm{ax}} - \hat{d}^{\mathrm{den}})\,\mathrm{d}u, \tag{11b}$$

$$\int C(\cdot,u)\,\Psi(u)\,\mathrm{d}u \simeq (\mathbb{1}_N - J)^{-1}\, K \left[\int \hat{C}(\cdot,u)\,(\Psi * \zeta)\,(u)\,\mathrm{d}u\right] \times K^{\mathbf{T}}\,(\mathbb{1}_N - J)^{-1\,\mathbf{T}}, \tag{11c}$$

where the arbitrary function Ψ is to be replaced by $W_{\pm}$ shifted by the corresponding delays in (5) and (7). The time variable t has been omitted (or replaced by $\cdot$) for vectors and matrices that evolve over time, as will be the case in the remainder of this paper. The superscript "$\mathbf{T}$" denotes the matrix transposition; $\mathbb{1}_N$ is the identity matrix of size N; $\mathbf{e}$ is the column vector with N elements all equal to one

$$\mathbf{e} := [1, \ldots, 1]^{\mathbf{T}}, \tag{12}$$

and likewise $\hat{\mathbf{e}}$ is a similar M-column vector.

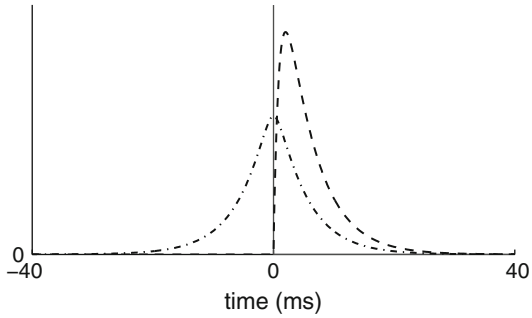

Fig. 6 Plots of ϵ (*dashed line*) and ζ (*dashed-dotted line*). Parameters are detailed in Appendix A

The function ζ is the self-convolution of the PSP kernel function ϵ (Gilson et al. 2009d, Sect. 2.3.4):

$$\zeta(r) := \int \epsilon(r + r')\epsilon(r')\,\mathrm{d}r'. \tag{13}$$

Figure 6 illustrates the functions ϵ and ζ for the parameters summarized in Appendix A. Combining (11b) with (5) and (11c) with (7), the covariance coefficients are now associated with

$$F_{ik}^{\Psi} \leftrightarrow \int \hat{C}_{kl}(\cdot,u)\,[\Psi * \epsilon]\left(u - 2\hat{d}^{\mathrm{den}}\right)\mathrm{d}u,$$
$$C_{ik}^{\Psi} \leftrightarrow \int \hat{C}_{kl}(\cdot,u)\,[\Psi * \zeta]\left(u + d^{\mathrm{ax}} - d^{\mathrm{den}}\right)\mathrm{d}u. \tag{14}$$

In our previous companion papers (Gilson et al. 2009a,d), the argument of both $\Psi * \epsilon$ and $\Psi * \zeta$ was just u. For delta-correlated inputs as described in (9), we define the following coefficients that correspond to the convolutions in the right-hand side (RHS) of (14):

$$\hat{C}_{kl}^{W_{\pm} * \epsilon} \simeq \hat{c}\,\hat{\nu}_0\,[W_{\pm} * \epsilon](-2\hat{d}^{\mathrm{den}}),$$
$$\hat{C}_{kl}^{W_{\pm} * \zeta} \simeq \hat{c}\,\hat{\nu}_0\,[W_{\pm} * \zeta](d^{\mathrm{ax}} - d^{\mathrm{den}}). \tag{15}$$

The consequence of taking the dendritic delays into account is that the argument of ζ can be negative in the new formulation. This will be of importance in the analysis of the weight specialization in Sect. 4.2. Note that the effect of dendritic delays in (15) is different for input and recurrent connections because of the approximations we have made.

In (11a–11c), the matrix J must have all its eigenvalues in the unit circle so that $\mathbb{1}_N - J$ is invertible at all times and thus the neuron firing rates do not diverge toward infinity; this issue is related to the choice of the Poisson neuron model (Gilson et al. 2009c, Appendix A) and corresponds to

non-saturated firing rate for realistic neurons. We also ignore autocorrelations in the present framework, assuming large numbers of external inputs and network neurons, $M \gg 1$ and $N \gg 1$, respectively. Matrix versions of the learning equations for additive STDP can be found in Gilson et al. (2009a,d).

4 Learning dynamics induced by weight-dependent STDP

Similar to previous studies (Gilson et al. 2009a,d, Sect. 3), we focus on the steady states of the firing rates and synaptic weights. The mathematical analysis is performed for an arbitrary network configuration, but it will be illustrated with a homogeneous recurrent network stimulated by two pools of external inputs with the same firing rate that have within-pool spike time correlations, as described in Fig. 1 and Sect. 2.4. We examine how STDP can generate "proper" weight specialization (cf. Sect. 2.3): stable mean incoming weight for each neuron away from the bounds and sufficiently strong competition that can split an initially homogeneous weight distribution in a meaningful manner. The motivation is that, if STDP can produce bimodal weight distribution, then it can also lead to milder specialization schemes.

4.1 Homeostatic equilibrium

First, we want to obtain the situation where the firing rate and the mean incoming weights ($K_{\rm av} := \sum_{i,k} K_{ik}/n^K$ and $J_{\rm av} := \sum_{i,j} J_{ij}/n^J$ for both input and recurrent connections, respectively) have reached an equilibrium for each neuron, denoted by *homeostatic equilibrium*. Individual weights may continue to change, though. A non-saturated stable mean incoming weight for each neuron allows effective weight specialization: the corresponding distribution can then be spread or even split to favor one or several synaptic pathways. In order to obtain specialization for both the input and recurrent weights, each set must experience a homeostatic equilibrium. When this is realized, the mean neuronal firing rate $\nu_{\rm av} := \sum_i \nu_i/N$ also stabilizes.

Neglecting the inhomogeneities between neurons, the consistency equation (11a) for the firing rates averaged over the network becomes

$$\nu_{\rm av} \simeq \frac{\nu_0 + n^K_{\rm av} K_{\rm av}\, \hat{\nu}_{\rm av}}{1 - n^J_{\rm av} J_{\rm av}}. \tag{16}$$

When further ignoring the covariance terms in the learning Eqs. (2) and (6), we obtain the following rate-based equations for the mean input and recurrent weights:

$$\dot{K}_{\rm av} \simeq \eta \left[w^{\rm in}\, \hat{\nu}_{\rm av} + w^{\rm out}\, \nu_{\rm av} + g(K_{\rm av})\, \hat{\nu}_{\rm av}\, \nu_{\rm av} \right], \tag{17a}$$

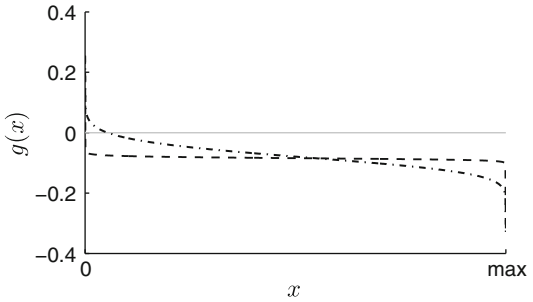

Fig. 7 Plots of g in (18), as a function of the weight, for $\gamma = 0.03$ (*dashed line*) and $\gamma = 0.1$ (*dashed-dotted line*), cf. Fig. 3b

$$\dot{J}_{\rm av} \simeq \eta \left[(w^{\rm in} + w^{\rm out})\, \nu_{\rm av} + g(J_{\rm av})\, \nu^2_{\rm av} \right], \tag{17b}$$

where $\hat{\nu}_{\rm av} := \sum_k \hat{\nu}_k/M$ is the mean input firing rate and we have defined, for the sake of simplicity,

$$g(x) := f_+(x)\, \widetilde{W}_+ - f_-(x)\, \widetilde{W}_-. \tag{18}$$

The function g is illustrated in Fig. 7 for various strengths of weight dependence and plays the role of $\widetilde{W}$ in our previous companion papers (Gilson et al. 2009a,d). For almost-additive STDP ($\gamma = 0.03$ in dashed line), g is roughly constant close to the value $\widetilde{W}_+ - \widetilde{W}_-$, except near the (soft) bounds; for medium weight dependence ($\gamma = 0.1$ in dashed-dotted line), g varies more gradually from $\widetilde{W}_+$ to $\widetilde{W}_-$. We now examine the fixed points ($\nu^*_{\rm av}$, $K^*_{\rm av}$, $J^*_{\rm av}$) of this dynamical system that must nullify the above expressions for $\dot{K}_{\rm av}$ and $\dot{J}_{\rm av}$ in (17a) and (17b). We will require a non-zero equilibrium value for the mean firing rate $\nu^*_{\rm av} > 0$.

4.1.1 *Influence of rate-based learning terms and weight dependence of STDP*

Case where $w^{\rm in} = w^{\rm out} = 0$. This has been previously studied for a single neuron (van Rossum et al. 2000; Gütig et al. 2003; Burkitt et al. 2004). From (17a) and (17b), we have

$$g(K^*_{\rm av}) = g(J^*_{\rm av}) = 0, \tag{19}$$

with g defined in (18). The equilibrium values of the mean weights, $K^*_{\rm av}$ and $J^*_{\rm av}$, only depend upon the function g; they are independent of the input firing rate $\hat{\nu}_{\rm av}$. The equilibrium value of the mean firing rate $\nu^*_{\rm av}$ for the neurons is then determined by (11a). For our STDP model, since $f_+(x) = f_-(J_{\max} - x)$ having a fixed point far from the soft bounds (around $J_{\max}/2$) implies either almost balanced STDP, i.e., $\widetilde{W}_+ \simeq \widetilde{W}_-$, or strong weight dependence ($\gamma > 0.1$).

Case where $w^{\rm in} \neq 0$ and/or $w^{\rm out} \neq 0$. The following necessary conditions must be satisfied in order to obtain equilibria for both the mean input and mean recurrent weights:

$$w^{\text{in}}\,\hat{\nu}_{\text{av}} + \left[w^{\text{out}} + g(K^*_{\text{av}})\,\hat{\nu}_{\text{av}}\right]\nu^*_{\text{av}} \simeq 0, \tag{20a}$$

$$w^{\text{in}} + w^{\text{out}} + g(J^*_{\text{av}})\,\nu^*_{\text{av}} \simeq 0. \tag{20b}$$

Except for particular values of the input and learning parameters, a non-zero equilibrium value ν^*_{av} for the mean firing rate implies

$$w^{\text{in}}\,g(J^*_{\text{av}})\,\hat{\nu}_{\text{av}} \simeq (w^{\text{in}} + w^{\text{out}})\left[w^{\text{out}} + g(K^*_{\text{av}})\,\hat{\nu}_{\text{av}}\right]. \tag{21}$$

In the case of additive STDP, for which the function $g(\cdot) = \widetilde{W}_+ - \widetilde{W}_-$ is constant, the equality (21) is never satisfied except for particular values of $\hat{\nu}_{\text{av}}$, w^{in}, and w^{out}. The specific case $w^{\text{out}} = 0$ will be discussed later in Sect. 4.1.3. Consequently, an equilibrium for both mean weights K_{av} and J_{av} cannot be attained. It is still possible to obtain a stable fixed point for ν_{av} in (16), but then the relationship

$$\dot{\nu}_{\text{av}} \simeq \frac{\partial \nu_{\text{av}}}{\partial K_{\text{av}}}\dot{K}_{\text{av}} + \frac{\partial \nu_{\text{av}}}{\partial J_{\text{av}}}\dot{J}_{\text{av}} \tag{22}$$

leads to K_{av} and J_{av} diverging in opposite directions (i.e., $\dot{K}_{\text{av}}\dot{J}_{\text{av}} < 0$) when (20a) and (20b) cannot be satisfied. This follows from

$$\begin{aligned}\frac{\partial \nu_{\text{av}}}{\partial K_{\text{av}}} &\simeq \frac{n^K_{\text{av}}\hat{\nu}_{\text{av}}}{1 - n^J_{\text{av}}J_{\text{av}}} > 0,\\ \frac{\partial \nu_{\text{av}}}{\partial J_{\text{av}}} &\simeq \frac{n^J_{\text{av}}\nu_{\text{av}}}{1 - n^J_{\text{av}}J_{\text{av}}} > 0.\end{aligned} \tag{23}$$

This rate-based competition between input and recurrent weights results in an inappropriate weight specialization. In other words, our model of additive STDP cannot lead to a homeostatic equilibrium when both input and recurrent connections are plastic.

For weight-dependent STDP, after using (16) and the equality (20a), we obtain the following constraint that allows us to express J^*_{av} in terms of K^*_{av}:

$$\begin{aligned}&w^{\text{in}}\,\hat{\nu}_{\text{av}}\left(1 - n^J_{\text{av}}J^*_{\text{av}}\right)\\ &\quad\simeq -\left[w^{\text{out}} + g(K^*_{\text{av}})\,\hat{\nu}_{\text{av}}\right]\left(\nu_0 + n^K_{\text{av}}K^*_{\text{av}}\,\hat{\nu}_{\text{av}}\right).\end{aligned} \tag{24}$$

Combining (21) and (24), the mean input weight K_{av} must be a zero of the following function h at the equilibrium:

$$h\left(K^*_{\text{av}}\right) \simeq 0 \tag{25}$$

with

$$\begin{aligned}h(K_{\text{av}}) :=\ &\left(w^{\text{in}} + w^{\text{out}}\right)\left[w^{\text{out}} + g(K_{\text{av}})\,\hat{\nu}_{\text{av}}\right] - w^{\text{in}}\,\hat{\nu}_{\text{av}}\\ &\times g\left\{\frac{1}{n^J_{\text{av}}} + \frac{\left[w^{\text{out}} + g(K_{\text{av}})\,\hat{\nu}_{\text{av}}\right]\left(\nu_0 + n^K_{\text{av}}K_{\text{av}}\,\hat{\nu}_{\text{av}}\right)}{w^{\text{in}}\,\hat{\nu}_{\text{av}}\,n^J_{\text{av}}}\right\}.\end{aligned} \tag{26}$$

Figure 8 illustrates the variations of h in (26) for weak weight dependence ($\gamma = 0.03$) and the corresponding equilibrium values of K^*_{av}, J^*_{av} and ν^*_{av} as a function of the mean input firing rate $\hat{\nu}_{\text{av}}$. Note that, for our choice of parameters (Appendix A), the function h is monotonically decreasing and thus has only one zero, synonymous with a unique fixed point $(\nu^*_{\text{av}}, K^*_{\text{av}}, J^*_{\text{av}})$. We observed that stronger weight dependence for STDP causes the fixed points K^*_{av} and J^*_{av} to be closer to $K_{\max}/2$ and $J_{\max}/2$, respectively. Then, $\hat{\nu}_{\text{av}}$ has less effect upon the equilibrium values, and because of (16), the equilibrium value ν^*_{av} becomes an almost linearly increasing function of $\hat{\nu}_{\text{av}}$, see Fig. 9.

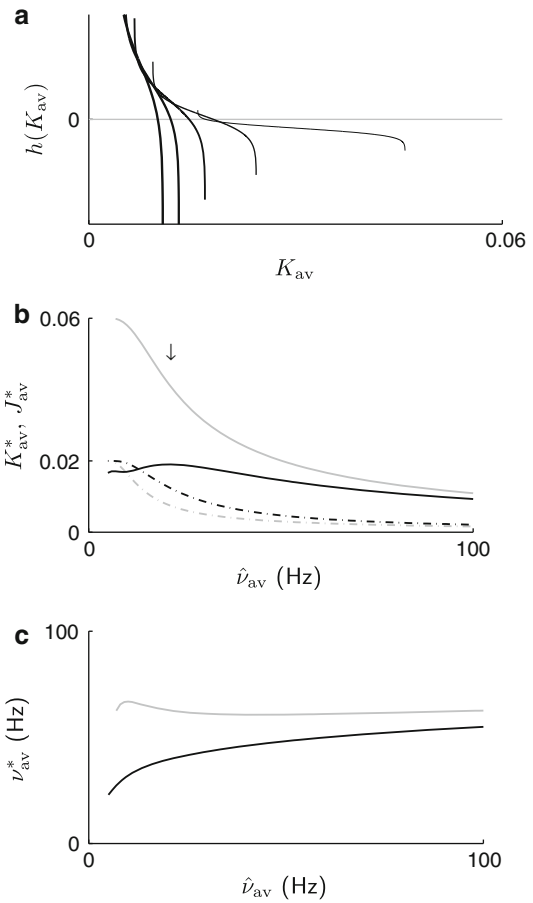

Fig. 8 Influence of *weak* weight dependence for STDP upon the homeostatic equilibrium. The plots correspond to $\gamma = 0.03$, the *dashed line* in Fig. 3b. **a** Plots of the function h in (26) for $\hat{\nu}_{\text{av}} = 10, 30, 50, 70,$ and 90 Hz (*thin-to-thick lines*). The zero of h when crossing the origin (*gray dashed line*) corresponds to the equilibrium value K^*_{av}. The plot is also restricted to the domain of K_{av} for which the value J_{av} given by (24) is within the bounds. **b** Equilibrium mean weights K^*_{av} (*solid line*) and J^*_{av} (*dashed-dotted line*) as functions of the input firing rate $\hat{\nu}_{\text{av}}$. The *black lines* correspond to (20a) and (20b) that ignore correlations, while the *gray lines* refer to (35) that incorporate the correction for the mean spike-time correlation, here $\hat{c}_{\text{av}} = 0.25$. The *arrow* indicates $\hat{\nu}_{\text{av}} = 20$ Hz as used in numerical simulation below. **c** Equilibrium value for the neuronal firing rate ν^*_{av} (*black line*) as a function of the input firing rate $\hat{\nu}_{\text{av}}$. Similar to **b**, the *gray line* takes the correlation into account. We used $N = M = 100$ with 30% connectivity and different upper bounds for the weights: $K_{\max} = 0.06$ and $J_{\max} = 0.02$; see Appendix A for details about other parameters

In order to obtain a realizable fixed point, which means a positive value for ν^*_{av}, the following additional necessary condition derived from (20a) and (20b) must also be satisfied

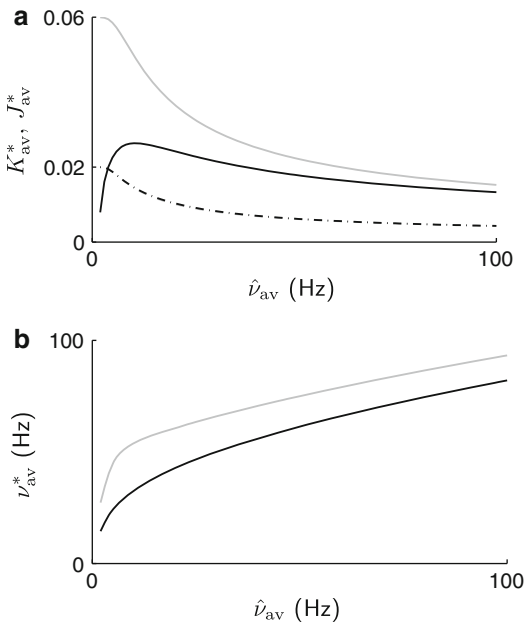

Fig. 9 Influence of *medium* weight dependence for STDP upon the homeostatic equilibrium. The plots (**a**) and (**b**) are the same as described for Fig. 8b and c, respectively, for medium weight dependence ($\gamma = 0.1$) corresponding to the dashed-dotted line in Fig. 3b

$$\nu^*_{av} \simeq -\frac{w^{in}\,\hat{\nu}_{av}}{w^{out} + g(K^*_{av})\,\hat{\nu}_{av}} \simeq -\frac{w^{in} + w^{out}}{g(J^*_{av})} > 0. \quad (27)$$

4.1.2 Stability of homeostatic equilibrium

In the absence of the rate-based terms w^{in} and w^{out}, the stability is determined by the derivatives $g'(K^*_{av})$ and $g'(J^*_{av})$: negative values ensure a stable homeostatic equilibrium for any level of input stimulation.

In the presence of w^{in} and w^{out}, the stability of fixed point $(\nu^*_{av}, K^*_{av}, J^*_{av})$ is given by a Jacobian matrix expressed using the partial derivatives of G and H that correspond to the RHS of (17a) and (17b), where we ignore the learning rate:

$$\begin{aligned} G(K_{av}, J_{av}) &:= \left[w^{in}\,\hat{\nu}_{av} + w^{out}\,\nu_{av} + g(K_{av})\,\hat{\nu}_{av}\,\nu_{av}\right], \\ H(K_{av}, J_{av}) &:= \left[\left(w^{in} + w^{out}\right)\,\nu_{av} + g(J_{av})\,\nu^2_{av}\right], \end{aligned} \quad (28)$$

where $\nu_{av} = \nu_{av}(K_{av}, J_{av})$ is an implicit function of K_{av} and J_{av}, cf. (16). The Jacobian matrix can then be expressed as

$$\begin{pmatrix} \frac{\partial G}{\partial K_{av}}(K^*_{av}, J^*_{av}) & \frac{\partial G}{\partial J_{av}}(K^*_{av}, J^*_{av}) \\ \frac{\partial H}{\partial K_{av}}(K^*_{av}, J^*_{av}) & \frac{\partial H}{\partial J_{av}}(K^*_{av}, J^*_{av}) \end{pmatrix} =: \begin{pmatrix} \alpha_1 & \alpha_2 \\ \alpha_3 & \alpha_4 \end{pmatrix}, \quad (29)$$

where

$$\alpha_1 = -w^{in}\frac{n^K_{av}\hat{\nu}^2_{av}}{(1 - n^J_{av}J^*_{av})\,\nu^*_{av}} + g'(K^*_{av})\,\hat{\nu}_{av}\,\nu^*_{av},$$

$$\begin{aligned} \alpha_2 &= -w^{in}\frac{n^J_{av}\hat{\nu}_{av}}{1 - n^J_{av}J^*_{av}}, \\ \alpha_3 &= -(w^{in} + w^{out})\frac{n^K_{av}\hat{\nu}_{av}}{1 - n^J_{av}J^*_{av}}, \\ \alpha_4 &= -(w^{in} + w^{out})\frac{n^J_{av}\nu^*_{av}}{1 - n^J_{av}J^*_{av}} + g'(J^*_{av})(\nu^*_{av})^2. \end{aligned} \quad (30)$$

We have used the equalities in (20a), (20b), and (23).

Stability of the mean weights K^*_{av} and J^*_{av} implies that of ν^*_{av} and requires that the Jacobian matrix has eigenvalues with negative real parts. In other words, the trace of the Jacobian matrix must be negative and the determinant must be positive in order to obtain stability, namely

$$\begin{aligned} &\alpha_1 + \alpha_4 < 0 \\ &\alpha_1\alpha_4 - \alpha_2\alpha_3 > 0. \end{aligned} \quad (31)$$

We require the stronger conditions $\alpha_1 < 0$ and $\alpha_4 < 0$ to ensure stability for the weight dynamics when either the input or the recurrent weights are plastic, while the other set of weights remains fixed. The following conditions are thus sufficient to ensure stability for any mean input firing rate $\hat{\nu}_{av}$:

$$\begin{aligned} &w^{in} + w^{out} > 0 \\ &w^{in} > 0 \\ &g' < 0. \end{aligned} \quad (32)$$

Note that the last condition $g' < 0$ is satisfied for any choice of $0 \le \gamma \le 1$ in our model of weight-dependent STDP, cf. Fig. 7. The condition for a realizable equilibrium in (27) must also be satisfied; when combined with (32), we obtain

$$\begin{aligned} &w^{out} + g(K^*_{av})\,\hat{\nu}_{av} < 0, \\ &g\left(J^*_{av}\right) < 0. \end{aligned} \quad (33)$$

This means, in particular, that g is required to be negative on a substantial support. The present stability analysis agrees with previous analytical studies of a homogeneous fixed point in the weight dynamics (Gütig et al. 2003; Meffin et al. 2006). Note that from our previous results for additive STDP, where $g' = 0$, the conditions in (33), that are satisfied for $g(\cdot) = \widetilde{W}_+ - \widetilde{W}_- < 0$, were sufficient to obtain a realizable stable homeostatic equilibrium for any value of $\hat{\nu}_{av}$ for either plastic input weights or plastic recurrent weights (Gilson et al. 2009a,d).

Under the above conditions (32) and (33), the equilibrium values K^*_{av} and J^*_{av} may still depend upon $\hat{\nu}_{av}$ in a complex fashion. However, after rewriting (27) as

$$\nu^*_{av} \simeq -\frac{w^{in}}{\frac{w^{out}}{\hat{\nu}_{av}} + g(K^*_{av})}, \quad (34)$$

we find that, provided the equilibrium values for the mean weights are far from the bounds such that $g(K^*_{av})$ is roughly

constant, the condition $w^{\text{out}} < 0$ ensures that ν^*_{av} is an increasing function of $\hat{\nu}_{\text{av}}$, as illustrated by the black curves in Figs. 8c and 9b. Note that this conclusion is similar to the case of additive STDP applied only to plastic input connections (Gilson et al. 2009a); because of the the weight dependence, the neuronal firing rates are not constrained to an equilibrium value independent of the mean input firing rate, which differs from the result obtained for additive STDP applied only to plastic recurrent connections (Gilson et al. 2009c).

4.1.3 Effect of correlations on homeostatic equilibrium

The previous results assumed no input spike-time correlations. In order to take them into account, we use the following equations instead of (20a) and (20b):

$$\begin{aligned} &w^{\text{in}}\,\hat{\nu}_{\text{av}} + \left[w^{\text{out}} + g(K^*_{\text{av}})\,\hat{\nu}_{\text{av}}\right]\nu^*_{\text{av}} \\ &\quad + \left(\hat{C}^{W_+ * \epsilon}_{\text{av}} - \hat{C}^{W_- * \epsilon}_{\text{av}}\right)\frac{n^K_{\text{av}} K^*_{\text{av}}}{1 - n^J_{\text{av}} J^*_{\text{av}}} \simeq 0, \\ &(w^{\text{in}} + w^{\text{out}})\nu^*_{\text{av}} + g(J^*_{\text{av}})\,(\nu^*_{\text{av}})^2 \\ &\quad + \left(\hat{C}^{W_+ * \zeta}_{\text{av}} - \hat{C}^{W_- * \zeta}_{\text{av}}\right)\left(\frac{n^K_{\text{av}} K^*_{\text{av}}}{1 - n^J_{\text{av}} J^*_{\text{av}}}\right)^2 \simeq 0. \end{aligned} \tag{35}$$

Here, we have used the approximations for the mean covariance coefficients $F^{W_\pm}_{\text{av}}$ and $C^{W_\pm}_{\text{av}}$ by averaging (11b) and (11c) over the network, which gave the last terms in each left-hand side (LHS) of (35), cf. (15). Note that, with additive STDP, setting $w^{\text{out}} = 0$ does not reduce the two equations to a single one, in contrast to the more approximated version in (20a); this means that additive STDP does not have a solution to both equations in (35) in general.

Now we consider weight-dependent STDP that can stabilize mean weights for both input and recurrent connections. The terms involving $\hat{C}$ in (35) depend upon the mean input correlation $\hat{c}_{\text{av}}$, as described in Sect. 2.4 and (15). For small values of $\hat{c}_{\text{av}}$, the extra terms in (35) compared with (20a) and (20b) do not modify the stability of the dynamical system for small correlation strengths when the conditions in (32) are satisfied. In this case, the extra terms can indeed be seen as "perturbations" that are smaller in magnitude compared to the rate-based terms in (17a) and (17b). Larger values for $\hat{c}_{\text{av}}$ may affect the stability, but this will not be further analytically investigated here. It turns out, however, that the equilibrium values are very sensitive to the mean input correlation, as illustrated in Fig. 8b: the new predictions with corrections (gray lines) are dramatically different from those obtained in Sect. 4.1.1 (black lines). The mean neuronal firing rate is thus also affected by the corrections, with correlated inputs leading to a higher equilibrium value, see Fig. 8c. The discrepancies vanish for higher input firing rate $\hat{\nu}_{\text{av}}$. Stronger weight dependence diminishes the effect of correlations without eliminating them, as illustrated in Fig. 9.

Figure 10 corroborates the sensitivity of the above-mentioned equilibrium values to the mean input correlation for almost-additive STDP. The simulated means (thick solid lines) are far from the predicted values when the correlations are ignored (dotted lines). During the first stage of the simulation, the mean weights evolve toward the corrected predictions when the input correlations are incorporated (dashed lines), cf. the arrow in Fig. 8b. After a while, when the weight specialization becomes effective, the mean weights then (slightly) diverge from the respective equilibrium values. Discrepancies with respect to the theoretical predictions are then mainly due to the emerging inhomogeneities in the weights, but also arise from those among input correlations (i.e., two pools) and partial connectivity.

4.2 Emergence of weight structure with correlated inputs

Now we assume the homeostatic equilibrium to be satisfied and we examine the emergence of weight structure within the input and recurrent plastic connections. In the learning equations (2) and (6), the rate-based terms almost cancel each other at the equilibrium when the input firing rates are almost homogeneous. Consequently, the terms related to the spike-time covariances (involving F and C) thus become the leading order. The way in which these terms generate effective weight specialization is similar to that for additive STDP. Different sets of weights diverge from each other such that an initially homogeneous weight distribution may become asymptotically bimodal (Gilson et al. 2009a,d). The details of $W_\pm$ do not matter in the specialization of the input weights provided the corresponding STDP is Hebbian and the conditions (32) are satisfied (Gilson et al. 2009a, Discussion). However, the evolution of the recurrent weights crucially depends upon the interplay between $W_\pm$, the recurrent delays, and the PSP kernel ϵ via the function ζ defined in (13): converse trends can be obtained depending upon these parameters (Gilson et al. 2009d, Discussion). For recurrent connections, the network structure relates to the distribution of the outgoing weights, while the incoming weights are constrained via their mean by the homeostatic equilibrium. The weight evolution can be predicted using the evaluation of the covariance coefficients in the learning equations (2) and (6). As a general rule of thumb, weights that correspond to $F^{W_+}_{ik} - F^{W_-}_{ik}$ and $C^{W_+}_{ij} - C^{W_-}_{ij}$ that are more positive will be potentiated at the expense of others.

For delta-correlated inputs (Sect. 2.4), the matrices $F^{W_+} - F^{W_-}$ and $C^{W_+} - C^{W_-}$ can be expressed in terms of the coefficients in (15). Recall that we assumed almost identical dendritic and axonal delays for each set of input and recurrent connections (Sect. 3.2). Since the function $W_- * \epsilon$ is zero for negative arguments, we always have $[(W_+ - W_-) * \epsilon](-2\hat{d}^{\text{den}}) > 0$, which ensures the potentiation of the

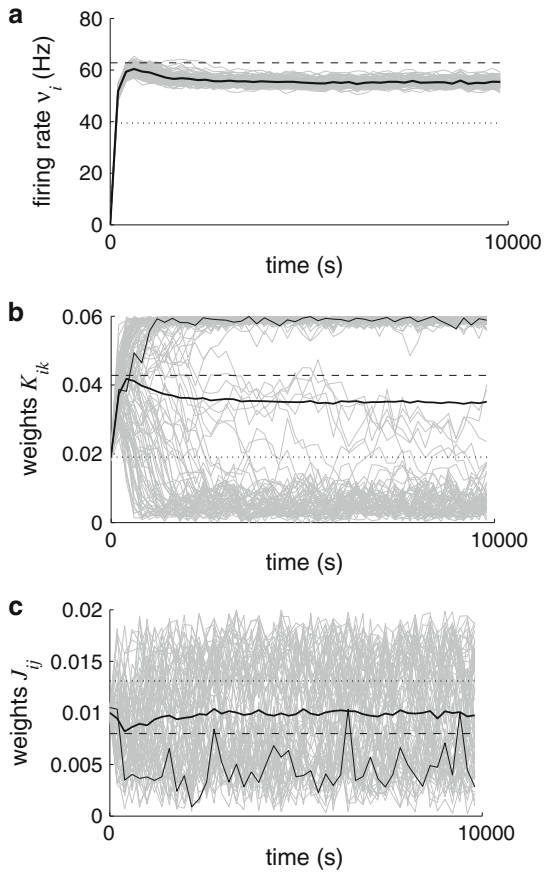

Fig. 10 Evolution of the **a** firing rates, **b** input, and **c** recurrent plastic weights due to STDP. Only a portion of the weights is represented. Almost-additive STDP corresponding to $\gamma = 0.03$ was used. The simulated network consisted of $N = 100$ neurons that received excitation from two pools of $M/2 = 50$ inputs each. Partial connectivity was generated by randomly assigning connections with probability 50% for input connections and 30% for recurrent connections. The two pools had the same firing rate 20 Hz and intra-pool correlation level $\hat{c}_1 = \hat{c}_2 = 0.25$, which corresponds to 50% synchronous spikes for any pair of correlated inputs. All initial weights were homogeneous. In each plot, the gray bundles represent individual firing rates or weights (only a portion is represented), one particular trace in each plot has been drawn for purposes of illustration in *black thin solid line*, and the *thick solid lines* are the corresponding means over the whole network. The theoretical predictions indicated in *dashed lines* incorporate the mean input correlation (Sect. 4.1.3) while those in *dotted lines* ignore them (Sect. 4.1.1)

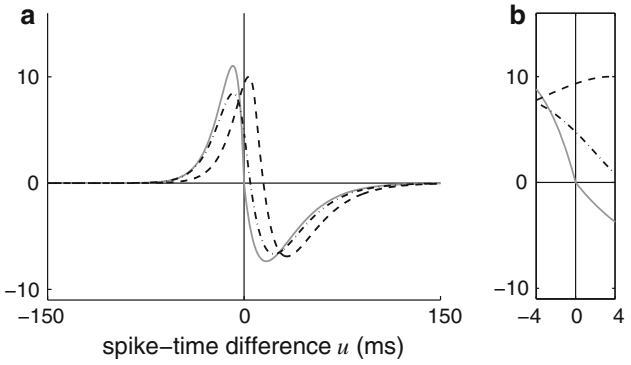

Fig. 11 **a** Plots of $W_+ - W_-$ (*gray solid line*), $(W_+ - W_-) * \epsilon$ (*dashed line*) and $(W_+ - W_-) * \zeta$ (*dashed-dotted line*). Globally, the shapes of the three functions are similar, apart from differences for small $u > 0$: $[W_+ - W_-](u) < 0$, whereas $[(W_+ - W_-) * \epsilon](u) > 0$ and $[(W_+ - W_-) * \zeta](u) > 0$ with our choice of parameters (Appendix A), see inset **b**. The impact of delta-correlated inputs relates to these values close to the origin

synaptic pathways coming from the more correlated input pools. However, the shape of the curve $(W_+ - W_-) * \zeta$ around the origin depends on the value of W_+ and W_- near the origin; strengthening of recurrent feedback connections within neuronal groups that receive correlated inputs was shown to require a positive value (Gilson et al. 2009d, Sect. 4.2). The corresponding curves are illustrated in Fig. 11. The details of the recurrent delays play a significant role here: a predominant dendritic component is equivalent to shifting the curve of $W_\pm$ to the right, which ensures more positive values. In contrast, a larger axonal delay implies weaker positive or even negative values, for which STDP weakens recurrent feedback within neuronal groups; the situation for the non-shifted curve analyzed in that paper actually corresponds to purely axonal delays, which explains more clearly why very short recurrent delays were necessary in numerical simulation to obtain the desired weight specialization. In addition to the delays, the respective amplitudes of STDP at the origin also play a role and result in favoring self-feedback when potentiation exceeds depression for small values of u in Fig. 11, namely $c_P > c_D$ in Appendix A while keeping $\widetilde{W}_+ - \widetilde{W}_- = c_P \tau_P - c_D \tau_D < 0$ to obtain a stable homeostatic equilibrium.

For weight-dependent STDP to generate splitting similar to that of the additive version, the elements of the following matrices $f_+(K^*_{\text{av}})\, F^{W_+} - f_-(K^*_{\text{av}})\, F^{W_-}$ and $f_+(J^*_{\text{av}})\, C^{W_+} - f_-(J^*_{\text{av}})\, C^{W_-}$ must have the same corresponding signs as $F^{W_+} - F^{W_-}$ and $C^{W_+} - C^{W_-}$, respectively. This is indeed the case whenever the respective values of f_- and f_+ at each fixed point K^*_{av} and J^*_{av} are comparable, namely

$$\begin{aligned} f_-(K^*_{\text{av}}) &\sim f_+(K^*_{\text{av}}), \\ f_-(J^*_{\text{av}}) &\sim f_+(J^*_{\text{av}}). \end{aligned} \tag{36}$$

Other conditions may be derived for more specific cases, but we will focus here upon those that are sufficient for any general input correlation structure. Consequently, the initial splitting of the weights is not affected by the weight dependence of STDP when (36) is satisfied. In our model, this holds when the equilibrium values K^*_{av} and J^*_{av} are away from the bounds according to Fig. 3b. As illustrated in Fig. 9b for average weight-dependent STDP, most values of $\hat{\nu}_{\text{av}}$ fall within this case, the exception corresponding to low input firing

rates (below 10 Hz). However, almost-additive STDP may lead to fixed points K^*_{av} and J^*_{av} too close to the bounds; for example, see J^*_{av} for small values of $\hat{\nu}_{\mathrm{av}}$ with no correlations in Fig. 8b. Other choices for $f_\pm$ may prove useful to palliate this problem.

When splitting away from the mean equilibrium value (K^*_{av} and J^*_{av}, respectively), the evolution of individual weights is affected by the weight dependence. The latter implies soft lower and upper bounds such that the weights experience a graduated saturation toward either bound. Namely, strong weight dependence leads to weaker splitting of the weights and the weight distribution may actually remain unimodal; in contrast, almost-additive STDP performs strong weight specialization (Gütig et al. 2003).

In a simulation using almost-additive STDP (Fig. 10), the asymptotic distribution of input weights became bimodal whereas the recurrent weights remained apparently unimodal (even though spread), indicating less competition for the recurrent than the input connections. This can be related to the relative values of $[(W_+ - W_-) * \epsilon](-2\hat{d}^{\mathrm{den}})$ and $[(W_+ - W_-) * \zeta](d^{\mathrm{ax}} - d^{\mathrm{den}})$ in Fig. 11, in agreement with previous results using additive STDP and short, purely axonal delays (Gilson et al. 2009a,d). To examine the structure imposed by STDP, we consider, for each neuron i, the difference between the mean input weights from the first and second pools: $\bar{K}_{i1} - \bar{K}_{i2}$. Figure 12a illustrates the evolution of input selectivity for each neuron: 54% of the neurons specialized to input pool $\hat{1}$ (traces going up) and 46% to pool $\hat{2}$ (traces going down); these numbers may vary across simulations. This evolution is similar to that obtained for additive STDP when applied only to the input weights and relates to an unstable fixed point, hence a diverging behavior (Gilson et al. 2009b). When we label the neurons as groups 1 and 2 according to the input pool that they specialized to, the structure developed amongst the recurrent connections can be evaluated by considering $\bar{J}_{i1} - \bar{J}_{i2}$ for neuron i in group 1, where $\bar{J}_{ix}$ is the mean incoming weight of the connections from group x to neuron i, and likewise $\bar{J}_{i2} - \bar{J}_{i1}$ for neuron i in group 2. As shown in Fig. 12b, STDP favored the connections within each group and depressed those between the two groups (traces going up). In general, the specialization for recurrent weights only begins after obtaining sufficiently clear input selectivity (some hundreds of seconds here). This agrees with previous results where only the recurrent connections were plastic (with additive STDP) and the fixed input connections were already organized in a similar manner to the configuration obtained in Fig. 12a (Gilson et al. 2009d). At the end of the learning epoch, we obtain two groups of 54 and 46 neurons each, respectively, which are selective to a different input pool, as illustrated in Fig. 13a. The recurrent connections are also polarized in a way that reinforces feedback within each group, though less clearly, see Fig. 13b. This is confirmed by the respective histograms in Fig. 13c and d, where dark gray indicates connections that are predicted to be potentiated. In that simulation, the specialization for recurrent connections has an amplitude equal to half of that for the input connections, in terms of separating the mean weights (with respect to the weight bounds). The mean for the (predicted) potentiated recurrent weights is roughly equal to 69% of the upper weight bound, whereas that for depressed recurrent weights is about 28%; the strengthened recurrent pathways are about 2.5 times (40% of the weight span) stronger than the the weakened ones. Comparatively, the potentiated and depressed input weights have their means equal to 98% and 19%, respectively, of the corresponding upper bound (the difference corresponds to ∼80% of the weight span).

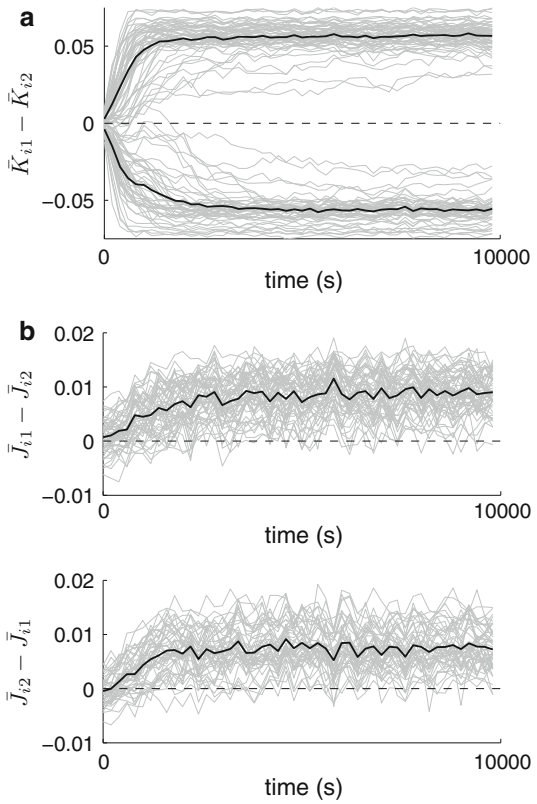

Fig. 12 Development of a structure amongst the **a** input and **b** recurrent weights due to STDP. The network is the same as Fig. 10. **a** Emergence of input selectivity. Each gray trace represents the difference between the mean input weights from the first and second pools. A first group of 54 neurons became selective to the first input pool (increasing curves), while a second group of 46 neurons did so to the second pool (decreasing curves). The *thick solid curves* indicate the mean weight differences for the two emerged neuronal groups. **b** Organization of the recurrent connections between the two emerged neuronal groups (one plot per group). Gray traces represent the difference between the mean recurrent weights from the same group (as neuron i) and the other group; the averages over all neurons from each group are represented in *thick solid lines*. Connections within each group were potentiated while those between the two groups were depressed (increasing curves)

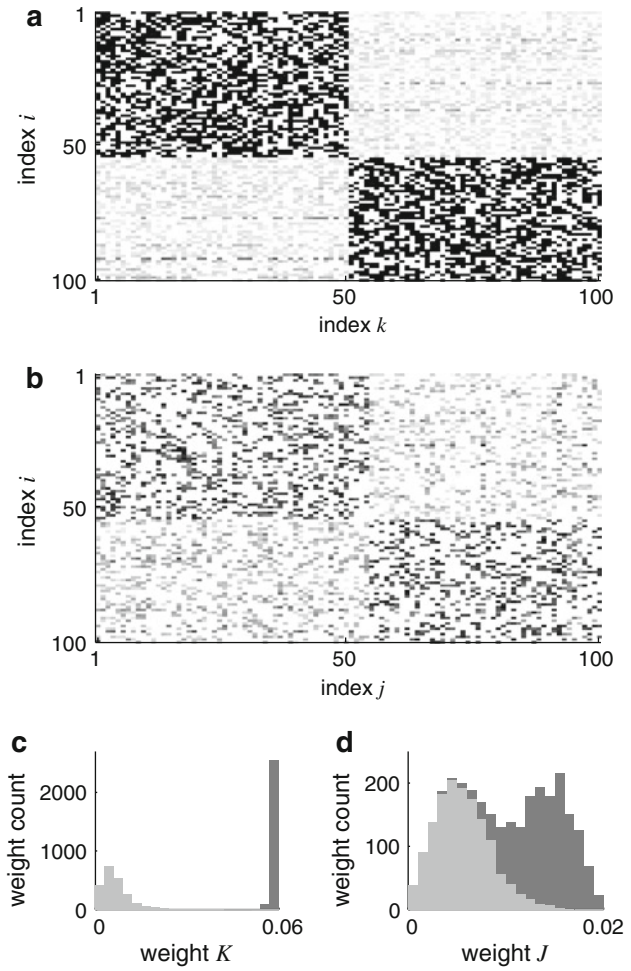

Fig. 13 Asymptotic weight matrices of the **a** input and **b** recurrent connections. The network is the same as Fig. 10. Darker pixels indicate potentiated weights. The indices of the neurons have been arranged according to which group they belong to: group 1 specialized to input pool $\hat{1}$ and group 2 to input pool $\hat{2}$. Note that the connectivity density is 50% for input connections and 30% for recurrent connections, respectively. **c**, **d** Respective histograms for input and recurrent connections. Dark gray indicates connections that are predicted to be potentiated, e.g. those coming from the first input pool to the first emerged neuronal group, and within-group recurrent connections

The stabilization of individual weights takes less time for input weights than for recurrent weights. As illustrated by the black thin solid lines representing the trace of a particular weight in Fig. 10b and c, the recurrent weight experiences large moves even after the significant population trend is established. However, recurrent weights remain either potentiated or depressed compared to the mean weight within their spread distribution, even though it is not clearly bimodal. Specialization by competition for recurrent weights is weaker compared to that for input weights, as indicated by the respective values of $(W_+ - W_-) * \epsilon$ and $(W_+ - W_-) * \zeta$ in Fig. 11b. Another point is that the function ϵ is non-zero only for positive arguments, cf. Fig. 6, so delta-correlated inputs lead to a systematic drive for input connections. In contrast, ζ is symmetrical, and the weight modifications induced by STDP are contradictory in the sense that they involve both systematic potentiation and depression due to the correlations between pre- and post-synaptic spikes. Consequently, the learning dynamics induces increased "stochastic noise" for recurrent weights than input weights. This phenomenon weakens the weight specialization and is stronger when using a relatively fast learning rate (here $\eta \sim 10^{-4}\, K_{\max}$ and $J_{\max}$).

Denser recurrent connectivity tends to prevent the emergence of two groups (Gilson et al. 2009b,c), while stronger input correlation favors the splitting of weights: these two phenomena compete with each other to determine the weight specialization. For the example of two input pools with $\hat{c} = 0.1$ (not shown here), the observed self-organization was much weaker. Increasing weight dependence also prevents the weights from splitting and simulations using $\gamma = 0.1$ and $\hat{c} = 0.25$ (not shown here) did not exhibit significant weight specialization, but rather unimodal asymptotic distributions around the corresponding equilibrium values for the means for both the input and recurrent weights.

As mentioned earlier, similar results can also be obtained without rate-based terms: $w^{\text{in}} = w^{\text{out}} = 0$. With our STDP model, however, this implies medium (or stronger) weight dependence and almost balanced ratio between potentiation and depression ($\widetilde{W} \sim 0$) such that K^*_{av} and J^*_{av} are away from the weight bounds, and (36) is satisfied too. Here, the use of w^{in} and w^{out} ensures suitable conditions for a broader range of STDP parameters. Other choices for the scaling functions $f_\pm$ can lead to both homeostatic equilibrium determined by (19) and effective weight specialization (Meffin et al. 2006). The emerging network structure may be jeopardized when using too strong weight dependence for STDP that results in a narrow unimodal weight distribution.

4.3 Retaining the weight structure with uncorrelated inputs

The previous section showed how a weight structure can emerge depending on correlated stimulation. When the external inputs have no spike-time correlations, a desirable effect is to preserve a pre-existent structure that has been imposed upon the network by a previous learning epoch. In a previous companion paper, we showed that additive STDP does not erase all information contained in recurrent connections that are already organized (Gilson et al. 2009c, Sect. 4.2). Now we examine this phenomenon with weight-dependent STDP through two examples using numerical simulation.

First, our version of STDP did not split an initially unimodal distribution (even though the distributions became more spread), both for the input and recurrent weights, as illustrated in Fig. 14. Neurons did not specialize to one or the other input pool despite using almost-additive STDP ($\gamma = 0.03$), see Fig. 10b for a comparison. The recurrent

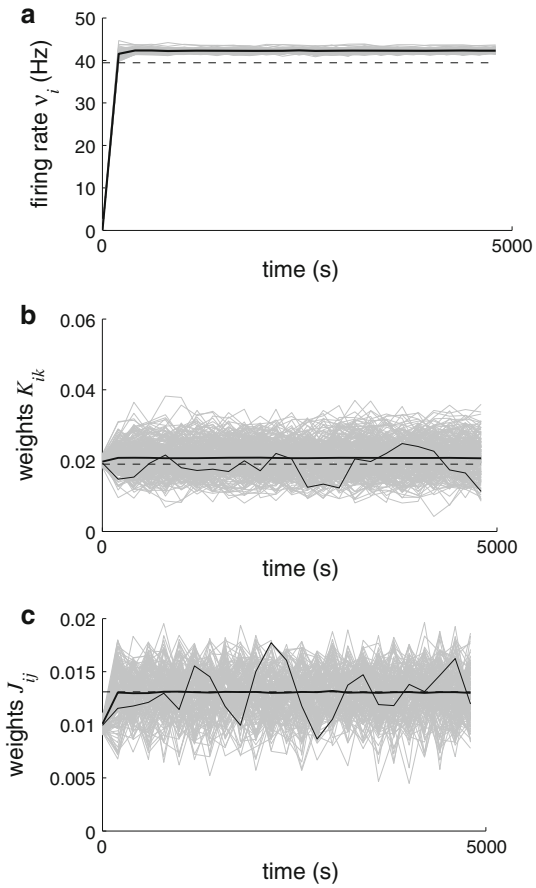

Fig. 14 Evolution of the **a** firing rates, **b** input, and **c** recurrent plastic weights due to almost-additive STDP ($\gamma = 0.03$). The simulated network is the same as in Fig. 10 with $N = 100$ neurons that receive excitation from two uncorrelated pools of $M/2 = 50$ inputs each, i.e. $\hat{c}_1 = \hat{c}_2 = 0$. All initial weights were homogeneous. The respective means (*thick solid lines*) stabilize close to the predicted values (*dashed lines*) calculated in Sect. 4.1.1. The *thin solid lines* illustrate the time courses of individual weights

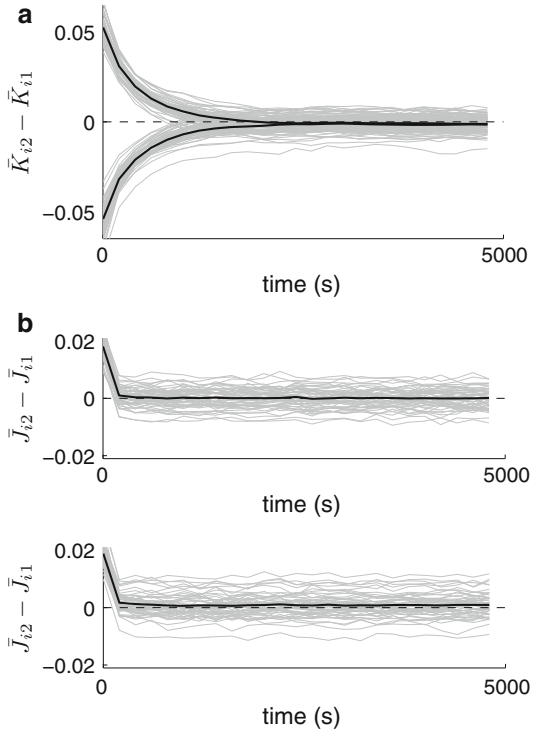

Fig. 15 Evolution of the structure among the **a** input and **b** recurrent connections for the same network as Fig. 14, except for the initial connectivity that is already organized similar to Fig. 17b. The plots are similar to Fig. 12, and the mean for each weight subset is represented in *thick solid line*

weights became spread in a weaker manner than in Fig. 10c and they did not exhibit any significant structure at the end of the learning epoch. Within the stable distribution, individual weights were constantly shuffled, as illustrated for the time course of individual weights indicated by the black solid lines in Fig. 14. The small discrepancies with respect to the theoretical predictions (black dashed lines) stem from autocorrelations and partial connectivity. A similar behavior has been shown in previous studies for recurrently connected neurons and stronger weight dependence (Morrison et al. 2007).

Second, we used a network configuration that is initially already organized and reproduces the organization obtained in Sect. 4.2, as sketched in Fig. 17b. In that simulation, STDP caused the network to gradually "forget" the previously learned weight specialization for the input connections (within 2000 s), but the recurrent connections almost immediately became homogeneous (less than 200 s), as illustrated in Fig. 15. This is in contrast with our previous results using additive STDP to train recurrent weights with fixed input connections, for which some qualitative features of the initial weight distributions were preserved throughout the learning epoch (Gilson et al. 2009a,c). It seems that the corresponding fixed-point manifold of dimension $n^J - N$ obtained for additive STDP is reduced to a point where all weights are equal to the same value J^*_{av} for weight-dependent STDP. Here, the persistence of the initial organization is primarily determined by the learning rate, but it is also affected by the strength of the weight dependence.

4.4 Emergence of weight structure for inhomogeneous firing rates

Finally, we evaluate the influence of inhomogeneous input firing rates $\bar{\nu}_1$ and $\bar{\nu}_2$ upon the homeostatic equilibrium for the network configuration in Fig. 1. The aim is to gain insight into the resulting weight specialization; we do not consider spike-time correlations in the following analysis, which is similar to that in Sect. 4.1.1. Reformulating the fixed-point equations for the mean weights (20a) and (20b) together with the firing-rate consistency equation (16) by considering separately the mean weights $\bar{K}_1$ and $\bar{K}_2$ over each input pool, we have

$$0 \simeq w^{\text{in}}\,\bar{\hat{\nu}}_x + \left[w^{\text{out}} + g(\bar{K}_x^*)\,\bar{\hat{\nu}}_x\right]\nu_{\text{av}}^*, \tag{37a}$$

$$0 \simeq w^{\text{in}} + w^{\text{out}} + g(J_{\text{av}}^*)\,\nu_{\text{av}}^*, \tag{37b}$$

$$\nu_{\text{av}}^* \simeq \frac{\nu_0 + n_1^K \bar{K}_1^* \bar{\hat{\nu}}_1 + n_2^K \bar{K}_2^* \bar{\hat{\nu}}_2}{1 - n_{\text{av}}^J J_{\text{av}}^*}, \tag{37c}$$

where $x = 1, 2$ is the index of the input pool and n_1^K and n_2^K are the numbers of input connections, assumed to be equal to $n_{\text{av}}^K/2$ although we keep the more general expression here. In particular, (37a) for both $\bar{K}_1$ and $\bar{K}_2$ implies the following equilibrium condition after eliminating ν_{av}^*:

$$\left[g(\bar{K}_1^*) - g(\bar{K}_2^*)\right]\bar{\hat{\nu}}_1\,\bar{\hat{\nu}}_2 \simeq w^{\text{out}}\left(\bar{\hat{\nu}}_1 - \bar{\hat{\nu}}_2\right). \tag{38}$$

For a monotonic decreasing function g such as that used throughout this paper, (38) means that the condition $w^{\text{out}} < 0$ will induce an equilibrium in which a higher input firing rate $\bar{\hat{\nu}}_x$ is favored and leads to a larger value for $\bar{K}_x^*$, in a similar way to K_{av}^* (Gilson et al. 2009a). On the other hand, the influence of the inhomogeneities in the input firing rates vanishes for $w^{\text{out}} = 0$. Note that weight dependence is necessary to obtain a solution for (38); otherwise (i.e., in the case of additive STDP), the resulting dynamics is divergent depending on w^{out} as described above. Further analysis is left to subsequent papers. Figure 16 shows plots of the numerical solution to (37a–37c) to illustrate the effect of the weight dependence when varying $\bar{\hat{\nu}}_1$, while $\bar{\hat{\nu}}_2 = 20$ Hz. There, $\bar{K}_1^*$ (solid line) is smaller than $\bar{K}_2^*$ (dashed line) for $\bar{\hat{\nu}}_1 < \bar{\hat{\nu}}_2$ since we have used $w^{\text{out}} < 0$; the converse holds for $\bar{\hat{\nu}}_1 > \bar{\hat{\nu}}_2$. The equilibrium value for the recurrent weights J_{av}^* is not substantially affected by the inhomogeneities in $\bar{\hat{\nu}}_x$. Medium weight dependence ($\gamma = 0.1$) tends to move the equilibrium values (gray curves) toward $K_{\max}/2$ and $J_{\max}/2$, respectively; it also results in smaller discrepancies between $\bar{K}_1^*$ and $\bar{K}_2^*$ than for $\gamma = 0.03$ (black curves), similar to the difference between Figs. 9a and 8b. The resulting equilibrium values for the mean neuronal firing rate ν_{av}^* (not shown here) increases with $\bar{\hat{\nu}}_1$, similar to Figs. 8c and 9b. When $w^{\text{out}} \neq 0$, inhomogeneous input firing rates can thus lead to input selectivity. However, this does not generate structure among the recurrent weights since neurons will all specialize in the same manner (Gilson et al. 2009d): after all weights have equilibrated, all neurons still receive the same overall homogeneous influx, in contrast to the specialization to one of the two input pools obtained with spike-time correlations.

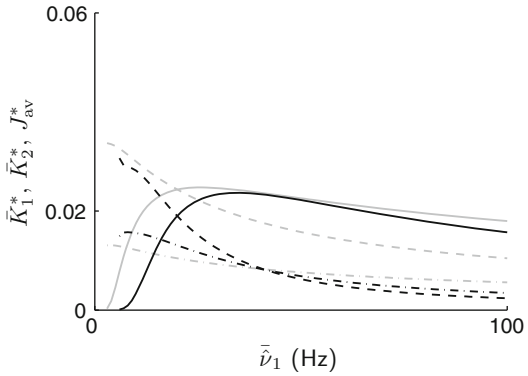

Fig. 16 Comparison between weak ($\gamma = 0.03$, in *black*) and medium ($\gamma = 0.1$, in *gray*) weight dependence for STDP upon the homeostatic equilibrium for unbalanced input firing rates. The curves represent the equilibrium values as a function of the mean input firing rate $\bar{\hat{\nu}}_1$ taken between 1 and 100 Hz, while $\bar{\hat{\nu}}_2 = 20$ Hz. Equilibrium values for the mean weights $\bar{K}_1^*$ (*solid line*), $\bar{K}_2^*$ (*dashed line*), and J_{av}^* (*dashed-dotted line*). We have used the same parameters as in Fig. 8 with $n_1^K = n_1^K = M/2 = 50$

5 Discussion

5.1 Spike-based versus rate-based learning

The results presented here have shown that STDP is capable of generating rich learning dynamics in recurrently connected networks, namely a mixture of partial stability and competition between individual synaptic weights, which can lead to robust neuronal specialization. These two complementary behaviors rely on the separation of time scales between rate effects and spike effects described in Sect. 2.3. In particular, the spike-driven effects play a central role in the emergence of a weight structure (Sect. 4.2).

The first dynamical ingredient of this weight specialization scheme relates to anti-Hebbian rate-based learning. A stable homeostatic equilibrium can be obtained for a wide range of learning parameters, when the recurrent connections are fixed (Gilson et al. 2009a), the input connections are fixed (Gilson et al. 2009c,d), or both are plastic (the present paper). By homeostatic equilibrium, we refer to the stability of the mean incoming weight for each neuron, applied to the two sets of input and recurrent connections (Sect. 4.1). The introduction of the rate-based terms (w^{in} and w^{out}) and/or weight dependence allows the use of unbalanced STDP: the function g defined in (18), which is the "mass" (i.e., aggregate effect) of STDP, needs only be negative on a substantial support according to (33), but is not necessarily tuned to be close to zero; this implies that STDP induces more overall depression than potentiation, hence its anti-Hebbian character. A necessary condition for the homeostatic stability in (32) concerns the rate-based term $w^{\text{in}} > 0$, which means that a sole pre-synaptic spike induces potentiation. The effect of a sole post-synaptic spike may be positive or negative, the choice $-w^{\text{in}} < w^{\text{out}} < 0$ leading to higher neuronal firing rates for stronger input stimulation. The influence of inhomogeneities in the input firing rates can be diminished by choosing $w^{\text{out}} \sim 0$. Without rate-based terms, stability can be obtained by choosing adequate functions $f_\pm$ to define the weight dependence (Meffin et al. 2006).

In our model, a specific issue concerns additive STDP: when learning modifies both input and recurrent weights, it is found that the two sets of weights diverge in opposite directions, until one of the sets reaches a bound. This phenomenon impairs any effective functional specialization in the network. Other simulation results (not presented) using different learning rates for the learning of input and recurrent connections did not solve this problem. For each neuron, competition between all incoming weights (of both types) is too strong for additive STDP, which potentiates one set of weights at the expense of the other. Weight dependence is then necessary to obtain stability via stable fixed points for both sets.

The above-mentioned conditions on the learning parameters ensure the existence of a fixed point that is stable and realizable, in the rate-based weight dynamics. These predictions are in agreement with earlier analytical studies for single neurons (Kempter et al. 1999; Gütig et al. 2003; Burkitt et al. 2004; Meffin et al. 2006), as well as numerical studies of integrate-and-fire neurons in feed-forward networks (Song et al. 2000) and recurrent networks (Song and Abbott 2001; Morrison et al. 2007). In particular, this prevents instability that may lead to the weights becoming either all quiescent or all saturated, as reported in numerical simulation, for example, by Song and Abbott (2001). Through the homeostatic equilibrium, we obtained synaptic scaling as a consequence of STDP alone (Kempter et al. 1999; Burkitt et al. 2007). The corresponding equilibrium values can be satisfactorily predicted by our framework (Sect. 4.1, cf. Figs. 10 and 14). The parameters w^{in}, w^{out}, and $\widetilde{W}_{\pm}$, together with $f_{\pm}$ and the weight bounds, can thus be chosen to tune the selectiveness of the network neurons as well as obtain equilibrium firing rates in a realistic range.

The second dynamical ingredient that drives the emergence of the weight structure is specific to spike-based learning. Neuron-to-input (resp. neuron-to-neuron) spike-time correlations can enforce a diverging behavior on input (recurrent) weights. Provided the homeostatic equilibrium remains satisfied and conditions in (36) are satisfied, it is not important how the homeostatic equilibrium is enforced (i.e., through rate-based terms and/or weight dependence). In order for the spike-based terms to become the leading order in the learning equations, it is necessary for the input spike-time correlations to be sufficiently strong. In the model used here (Gütig et al. 2003), "clear" weight specialization, such as a bimodal asymptotic distribution, requires relatively weak weight dependence (additive-like STDP). In contrast, medium or strong weight dependence produces unimodal asymptotic weight distribution. The specialization of recurrent connections requires, in addition, that the input connections are already "organized" (in an inhomogeneous manner), such that different network neurons do not all receive the same stimulation from the external inputs (Gilson et al. 2009d). Unbalanced input firing rates can lead to specialization of the weights via the rate-based homeostatic equilibrium, but this trend is overridden by the effect of spike-time correlations when the latter are sufficiently strong (Gilson et al. 2009a,d). In other words, the input correlation structure will dominate in determining the learning dynamics in the case of "not too strong" inhomogeneities in the firing rates. Further study is required to examine in more depth the case of "significantly" unbalanced input firing rates, in particular, the case where spike-time correlations and firing rates compete to impose opposite specializations. When inputs have no spike-time correlations, (even weakly) weight-dependent STDP can preserve an initially unimodal weight distribution (Sect. 4.3), as found in previous single neuron studies (van Rossum and Turrigiano 2001; Gütig et al. 2003; Morrison et al. 2007).

In our model, spike-time correlations correspond to coincident spiking within correlated input pools (Sect. 2.4). As an extension, any phenomenon corresponding to fast variations (order of milliseconds) of the firing probability for sufficiently many inputs is likely to induce a correlation structure, i.e., non-flat cross-correlogram $\hat{C}$. Examples include spike patterns (Masquelier et al. 2008), fast oscillations (Marinaro et al. 2007; Dahmen et al. 2008), and spike trains with given time-lag differences (Leibold et al. 2002); the subsequent weight specialization may, however, be substantially modified from that in the present analysis.

Another issue concerns the extension of our results to more elaborate and/or physiologically motivated forms of STDP. Temporal restrictions of the pairwise interactions that contribute to STDP (Sjöström et al. 2001) may change the homeostatic equilibrium (Burkitt et al. 2004), but should not impair the specialization related to spike-time correlations, since the contributions then correspond to pairs of near spikes for narrowly correlated spike trains. The introduction of spike triplets or higher interactions (Pfister and Gerstner 2006) may modulate the specialization scheme analyzed in Sect. 4. In contrast, the model proposed by Appleby and Elliott (2006) does not exhibit competition for pairs of spikes, but only higher-order interactions; our analysis does not apply to this learning rule. Likewise, more elaborate models of STDP involving more flexibility in the induced weight dynamics (Zou and Destexhe 2007; Graupner and Brunel 2007) should exhibit similar network dynamics when operating in a regime where they favor correlated pathways in a Hebbian fashion (recall that only excitatory glutamatergic-like synapses were considered in the present analysis).

5.2 Neuronal specialization leading to network structure

Our choice of pairwise STDP and the Poisson neuron model allowed us to determine the neuron-to-neuron and neuron-to-

input spike-time covariance structures in terms of the input-to-input structure (Sect. 3.2). The covariance consistency equations that we obtain allow us to determine the weight evolution. Our choice of learning rate η (Appendix A) leads to effective specialization in tens of minutes, which is persistent provided the input stimulus does not change. Our conclusions about the emerged structure hold for various speeds of learning, provided the input spike-time correlations have a significant effect on the learning dynamics. This may break down when the learning rate is increased, which induces stronger noise in the weight dynamics (Meffin et al. 2006). In terms of input specialization, STDP favors more correlated inputs provided it induces Hebbian spike-based learning, i.e., spikes taking part in the output firing induce an increase of the corresponding weight (Kempter et al. 1999; Gilson et al. 2009a). When a network is stimulated by two input pools with balanced spike-time correlations, this can lead to symmetry breaking with the emergence of two neuronal groups, each specialized to only one of the two pools (Song and Abbott 2001; Gütig et al. 2003; Gilson et al. 2009b). However, the evolution of plastic recurrent connections crucially depends upon the choice of parameters (Gilson et al. 2009d), which makes it possible to obtain more synchrony or decorrelation for neuronal groups (Iglesias et al. 2005; Lubenov and Siapas 2008; Câteau et al. 2008). More synchrony relates to the strengthening of within-group recurrent connections (Gilson et al. 2009d); in this case, STDP exhibits Hebbian spike-based learning. For delta-correlated input pools (Sect. 2.4), it requires STDP to induce stronger potentiation than depression for narrow spike-time correlations, as illustrated in Fig. 11. Together with the condition (33) for the homeostatic equilibrium, a suitable choice of $W_{\pm}$ involves a longer time constant for depression but higher amplitude for potentiation, in agreement with previous experimental results (Bi and Poo 1998). Under this condition, neuronal groups that receive stronger correlated inputs take over in the recurrent network (Song and Abbott 2001; Gilson et al. 2009d). Predominantly dendritic recurrent delays also favor within-group strengthening: they allow neurons with narrowly synchronized activity to potentiate synapses connecting them (Sect. 4.2), in agreement with previous studies (Senn 2002; Morrison et al. 2008). Inhomogeneous properties for the synapses would not modify the global conclusions presented here relative to equilibrium stability and specialization as they rely on qualitative properties, viz. signs of $(W_+ - W_-) * \in$ and $(W_+ - W_-) * \zeta$ around the origin. As highlighted earlier, weight dependence is necessary in our model of STDP to obtain a homeostatic equilibrium in the learning dynamics. To obtain a dramatic specialization such as splitting the distribution of afferent weights, our results favor a form of (weight-dependent) additive-like STDP. In contrast, stronger weight dependence produces unimodal distributions, which may be useful in other cases. Using different learning rates for input and recurrent connections was not found to affect the emerging structure, but only the speed of its development.

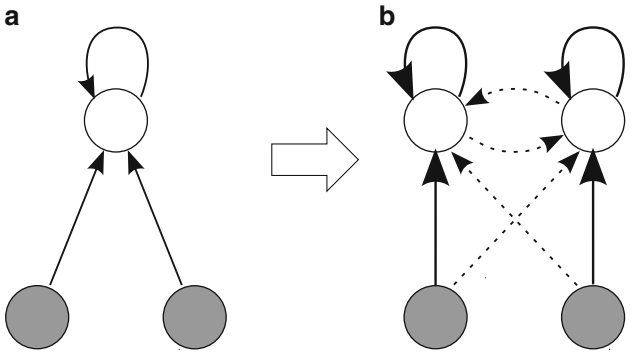

Fig. 17 Self-organization scheme in a network stimulated by two correlated pools of external inputs. The diagrams represent the connectivity **a** before and **b** after learning. Both input and recurrent connections are plastic. The initially homogeneous distribution of input weights is split by STDP and becomes bimodal such that two neuron groups emerge, each specialized to only one of the input pathways. The recurrent connections become structured such that within-group weights are potentiated at the expense of between-group weights. In **b**, *thick solid arrows* indicate potentiated weights and *dashed arrows* indicate depressed weights

In summary, we observed the emergence of specialized neuronal groups in an initially homogeneous recurrent network stimulated by two balanced correlated input pools, as illustrated in Fig. 17. We only assumed spike-time correlations between spike trains that belong to the same input pathway, but none otherwise. Our model of STDP alone generates the required dynamical ingredients to represent both input pathways in the weight structure (Sect. 4). In particular, no particular pre-existing connectivity topology and/or additional mechanisms is required to obtain the emergence of neuronal groups sensitive to one input pathway. Moreover, the resulting learning dynamics appears sufficiently robust to withstand to some extent (and it may even benefit from) the addition of refinements toward more physiologically realistic models that have been used, for example, in modeling the visual cortex (Malsburg 1973; Swindale 1996; Elliott and Shadbolt 1999; Goodhill 2007). The dynamical properties exhibited by STDP here may prove to be useful in such more elaborate models. In biology, other mechanisms such as structural plasticity that creates and eliminates synapses (Alvarez and Sabatini 2007; Butz et al. 2009; Holtmaat and Svoboda 2009) also occur in parallel to the waxing and waning of existing synapses, which interplays with the organization scheme presented here. The present analysis of learning dynamics may also have some bearing upon other plasticity rules adapted to bursty spike trains with a temporal learning window on the longer time scale (Butts et al. 2007). Such an organization scheme for ocular dominance in the primary visual cortex can be related to spontaneous retinal waves (Wong 1999; Butts et al. 2007), which implies a correlation input structure for some timescale (Gjorgjieva et al. 2009).

Our results may also be relevant for other systems with feedback connections using STDP, such as memory in the hippocampus (Neves et al. 2008).

5.3 Future directions

A systematic exploration using numerical simulation of the parameters associated with the PSP kernel, synaptic delays, and STDP temporal window is needed to verify the predictions in more depth, as well as the respective influence of the input firing rates and correlations. Other spiking neuron models, such as the integrate-and-fire neuron, may also modulate the present conclusions. Another analytical direction lies in considering longer time constants for the recurrent delays and the PSP kernel ϵ, in order to better understand the interplay between them and the STDP window function $W_{\pm}$, beyond the approximations detailed in Sect. 3.2.

It is not yet clear how rich a specialization STDP can generate upon synaptic weights within neuronal networks, especially when recurrent connections are involved or for heterogeneous synapses (e.g., for thalamocortical and intracortical pathways). More analytical progress is necessary in order to gain a better understanding of the unsupervised computational learning scheme performed by STDP. The main players involved in such information processing are the neuronal and synaptic mechanisms, structure of the stimulating inputs, network connectivity, and learning parameters. A global framework that incorporates numerous types of stimulating input structures (Delorme et al. 2001; Fusi 2002; Leibold et al. 2002; Dahmen et al. 2008; Masquelier et al. 2008) would be of great interest to gain a better understanding of the functional versatility assumed for generic cortical microcircuits. The present study also deliberately made minimal assumptions on the input correlation structure and network topology. The extent to which STDP generates and/or uses specific connectivity topology is still largely unknown. In this sense, the study of the learning dynamics in neuronal networks aims to link physiological modeling to machine learning.

Finally, the present series of papers, together with previous work (Gerstner et al. 1996; Kempter et al. 1999; Gütig et al. 2003), has shown that pairwise spike-time correlations are crucial for learning dynamics induced by a broad class of STDP models. This highlights the importance of spike-timing effects in neuronal information processing, and the learning window function determines the time scale at which they should be evaluated (Gerstner et al. 1993, 1996). Such group spiking properties (e.g., coincident firing) require sufficiently many neurons to be involved in order to have a significant effect on the learning dynamics. On a more general level, this relates to computation in a distributed fashion. Theoretical studies of spike-time correlations have just started to uncover their effect upon neuronal firing dynamics (Burkitt 2006; Moreno-Bote et al. 2008), but their role, a fortiori in vivo, is still largely unknown (Kriener et al. 2008; Renart et al. 2010). A better understanding of the interplay between spiking activity and synaptic plasticity in neuronal networks may contribute to this debate.

6 Erratum

In the first companion paper of this series (Gilson et al. 2009a), signs $<$ and $>$ were inverted between (ii) and (iii) at the top of the right column in page 9; they should read:

(ii) $\widetilde{W} < 0$ and $w^{\text{out}} > 0$: stable for $\hat{\nu}_{\text{av}} > -w^{\text{out}}/\widetilde{W}$;
(iii) $\widetilde{W} > 0$ and $w^{\text{out}} < 0$: stable for $\hat{\nu}_{\text{av}} < -w^{\text{out}}/\widetilde{W}$;

Acknowledgments The authors are greatly indebted to Chris Trengove, Sean Byrnes, Hamish Meffin, Michael Eager, and Paul Friedel for their constructive comments. They are also grateful to Iven Mareels, Konstantin Borovkov, Dragan Nesic, and Barry Hughes for earlier discussions. The authors are thankful to the Reviewers of the series of papers who contributed to improve the manuscripts. MG is funded by scholarships from the University of Melbourne and NICTA. MG also benefited from an enjoyable stay at the Physik Department (T35) of the Technische Universität München. LvH gratefully acknowledges a most enjoyable stay at the Department of Electrical and Electronic Engineering at the University of Melbourne. LvH is partially supported by the BCCN-Munich. Funding is acknowledged from the Australian Research Council (ARC Discovery Project #DP0771815). The Bionic Ear Institute acknowledges the support it receives from the Victorian Government through its Operational Infrastructure Support Program.

Appendix A: Simulation parameters

To illustrate our theoretical predictions, we simulated a network of $N = 100$ Poisson neurons that received excitation from two pools of $M/2 = 50$ external inputs; see Fig. 17a. Both the input and recurrent connectivity were partial and generated by randomly assigning connections with probability 30%. The timestep used was 10^{-4} s and weights in the plots were recorded every 200 s. The neuronal and learning parameters in Table 1 were used unless stated otherwise. The STDP window functions $W_{\pm}$ is defined by

$$\begin{aligned} W_+(u) &= c_P \frac{|u|}{\tau_P} \exp\left(-\frac{|u|}{\tau_P}\right) \quad \text{for } u < 0, \\ W_-(u) &= -c_D \frac{|u|}{\tau_P} \exp\left(-\frac{|u|}{\tau_D}\right) \quad \text{for } u > 0, \end{aligned} \tag{39}$$

with the constants c_P, τ_P, c_D, and τ_D in Table 1 chosen to obtain a profile similar to that for additive STDP used in the previous companion papers of the series (Gilson et al. 2009a,b,c,d).

Table 1 Table of simulation parameters

Time step	10^{-4} s
Simulation duration	10^4 s
Input Poisson spike trains	
Firing rates	$\hat{\nu}_{\text{av}} = 20$ Hz
Correlation level	$\hat{c} = 0 - 0.25$
Poisson neurons	
Instantaneous firing rate	$\nu_0 = 5$ Hz
Synapses	
Rise time constant	$\tau_A = 1$ ms
Decay time constant	$\tau_B = 5$ ms
Axonal input delays	$\hat{d}^{\text{ax}} = 1 \pm 1$ ms
Dendritic input delays	$\hat{d}^{\text{den}} = 4$ ms
Axonal recurrent delays	$d^{\text{ax}} = 1 \pm 1$ ms
Dendritic recurrent delays	$d^{\text{den}} = 4$ ms
STDP	
Learning parameter	$\eta = 5 \times 10^{-6}$
Pre-synaptic rate-based coefficients	$w^{\text{in}} = 4$
Post-synaptic rate-based coefficients	$w^{\text{out}} = -0.5$
Potentiation time constant	$\tau_P = 8.5$ ms
Potentiation scaling coefficient	$c_P = 30$
Depression time constant	$\tau_D = 17$ ms
Depression scaling coefficient	$c_D = 20$
Strength of weight dependence	$\gamma = 0\text{-}0.1$
Maximal input weight	$K_{\max} = 0.06$
Maximal recurrent weight	$J_{\max} = 0.02$

The PSP kernel ϵ is defined by

$$\epsilon(t) = \begin{cases} \frac{\exp(-t/\tau_B)-\exp(-t/\tau_A)}{\tau_B-\tau_A} & \text{for } t \geq 0 \\ 0 & \text{for } t < 0 \end{cases}. \tag{40}$$

These parameters are in the same range as those used in previous studies (Kempter et al. 1999; Burkitt et al. 2007).

References

Alvarez VA, Sabatini BL (2007) Anatomical and physiological plasticity of dendritic spines. Annu Rev Neurosci 30:79–97

Appleby PA, Elliott T (2006) Stable competitive dynamics emerge from multispike interactions in a stochastic model of spike-timing-dependent plasticity. Neural Comput 18(10):2414–2464

Bell CC, Han VZ, Sugawara Y, Grant K (1997) Synaptic plasticity in a cerebellum-like structure depends on temporal order. Nature 387(6630):278–281

Bi GQ, Poo MM (1998) Synaptic modifications in cultured hippocampal neurons: Dependence on spike timing, synaptic strength, and postsynaptic cell type. J Neurosci 18(24):10464–10472

Bi GQ, Poo MM (2001) Synaptic modification by correlated activity: Hebb's postulate revisited. Annu Rev Neurosci 24:139–166

Bienenstock EL, Cooper LN, Munro PW (1982) Theory for the development of neuron selectivity—orientation specificity and binocular interaction in visual-cortex. J Neurosci 2(1):32–48

Boettiger CA, Doupe AJ (2001) Developmentally restricted synaptic plasticity in a songbird nucleus required for song learning. Neuron 31(5):809–818

Burkitt AN (2006) A review of the integrate-and-fire neuron model: I. Homogeneous synaptic input. Biol Cybern 95(1):1–19

Burkitt AN, Meffin H, Grayden DB (2004) Spike-timing-dependent plasticity: the relationship to rate-based learning for models with weight dynamics determined by a stable fixed point. Neural Comput 16(5):885–940

Burkitt AN, Gilson M, van Hemmen JL (2007) Spike-timing-dependent plasticity for neurons with recurrent connections. Biol Cybern 96(5):533–546

Butts DA, Kanold PO, Shatz CJ (2007a) A burst-based "Hebbian" learning rule at retinogeniculate synapses links retinal waves to activity-dependent refinement. PLoS Biol 5(3):651–661

Butts DA, Weng C, Jin J, Yeh CI, Lesica NA, Alonso JM, Stanley GB (2007b) Temporal precision in the neural code and the timescales of natural vision. Nature 449:92–95

Butz M, Wörgötter F, van Ooyen A (2009) Activity-dependent structural plasticity. Brain Res Rev 60(2):287–305

Caporale N, Dan Y (2008) Spike timing-dependent plasticity: a Hebbian learning rule. Annu Rev Neurosci 31:25–46

Câteau H, Kitano K, Fukai T (2008) Interplay between a phase response curve and spike-timing-dependent plasticity leading to wireless clustering. Phys Rev E 77(5):051909

Choe Y, Miikkulainen R (1998) Self-organization and segmentation in a laterally connected orientation map of spiking neurons. Neurocomputing 21(1–3):139–157

Dahmen JC, Hartley DE, King AJ (2008) Stimulus-timing-dependent plasticity of cortical frequency representation. J Neurosci 28(50):13629–13639

Dan Y, Poo MM (2006) Spike timing-dependent plasticity: from synapse to perception. Physiol Rev 86(3):1033–1048

Debanne D, Gahwiler BH, Thompson SM (1998) Long-term synaptic plasticity between pairs of individual CA3 pyramidal cells in rat hippocampal slice cultures. J Physiol (Lond) 507(1):237–247

deCharms RC, Zador A (2000) Neural representation and the cortical code. Annu Rev Neurosci 23:613–647

Delorme A, Perrinet L, Thorpe SJ (2001) Networks of integrate-and-fire neurons using rank order coding B: Spike timing dependent plasticity and emergence of orientation selectivity. Neurocomputing 38:539–545

Egger V, Feldmeyer D, Sakmann B (1999) Coincidence detection and changes of synaptic efficacy in spiny stellate neurons in vat barrel cortex. Nat Neurosci 2(12):1098–1105

Elliott T (2003) An analysis of synaptic normalization in a general class of Hebbian models. Neural Comput 15(4):937–963

Elliott T, Shadbolt NR (1999) A neurotrophic model of the development of the retinogeniculocortical pathway induced by spontaneous retinal waves. J Neurosci 19(18):7951–7970

Feldman DE (2000) Timing-based LTP and LTD at vertical inputs to layer II/III pyramidal cells in rat barrel cortex. Neuron 27(1):45–56

Froemke RC, Dan Y (2002) Spike-timing-dependent synaptic modification induced by natural spike trains. Nature 416(6879):433–438

Fusi S (2002) Hebbian spike-driven synaptic plasticity for learning patterns of mean firing rates. Biol Cybern 87(5–6):459–470

Gerstner W, Ritz R, van Hemmen JL (1993) Why spikes? Hebbian learning and retrieval of time-resolved excitation patterns. Biol Cybern 69(5–6):503–515

Gerstner W, Kempter R, van Hemmen JL, Wagner H (1996) A neuronal learning rule for sub-millisecond temporal coding. Nature 383(6595):76–78

Gilson M, Burkitt AN, Grayden DB, Thomas DA, van Hemmen JL (2009a) Emergence of network structure due to spike-timing-dependent plasticity in recurrent neuronal networks I: input

selectivity–strengthening correlated input pathways. Biol Cybern 101(2):81–102
Gilson M, Burkitt AN, Grayden DB, Thomas DA, van Hemmen JL (2009b) Emergence of network structure due to spike-timing-dependent plasticity in recurrent neuronal networks II: input selectivity–symmetry breaking. Biol Cybern 101(2):103–114
Gilson M, Burkitt AN, Grayden DB, Thomas DA, van Hemmen JL (2009c) Emergence of network structure due to spike-timing-dependent plasticity in recurrent neuronal networks III: Partially connected neurons driven by spontaneous activity. Biol Cybern 101(5–6):411–426
Gilson M, Burkitt AN, Grayden DB, Thomas DA, van Hemmen JL (2009d) Emergence of network structure due to spike-timing-dependent plasticity in recurrent neuronal networks IV: structuring synaptic pathways among recurrent connections. Biol Cybern 101(5–6):427–444
Gjorgjieva J, Toyoizumi T, Eglen SJ (2009) Burst-time-dependent plasticity robustly guides ON/OFF segregation in the lateral geniculate nucleus. PLoS Comput Biol 5(12):e1000618
Goodhill GJ (2007) Contributions of theoretical modeling to the understanding of neural map development. Neuron 56(2):301–311
Goodhill GJ, Barrow HG (1994) The role of weight normalization in competitive learning. Neural Comput 6(2):255–269
Graupner M, Brunel N (2007) STDP in a bistable synapse model based on CaMKII and associated signaling pathways. PLoS Comput Biol 3(11):2299–2323
Gütig R, Aharonov R, Rotter S, Sompolinsky H (2003) Learning input correlations through nonlinear temporally asymmetric Hebbian plasticity. J Neurosci 23(9):3697–3714
Hawkes AG (1971) Point spectra of some mutually exciting point processes. J R Statist Soc Ser B 33(3):438–443
Hensch TK (2005) Critical period plasticity in local cortical circuits. Nat Rev Neurosci 6(11):877–888
Hirsch JA, Martinez LM (2006) Circuits that build visual cortical receptive fields. Trends Neurosci 29:30–39
Holtmaat A, Svoboda K (2009) Experience-dependent structural synaptic plasticity in the mammalian brain. Nat Rev Neurosci 10(9):647–658
Hubel DH, Wiesel TN (1962) Receptive fields, binocular interaction and functional architecture in cats visual cortex. J Physiol (Lond) 160(1):106–164
Iglesias J, Eriksson J, Grize F, Tomassini M, Villa A (2005) Dynamics of pruning in simulated large-scale spiking neural networks. Biosystems 79(1–3):11–20
Izhikevich EM, Desai NS (2003) Relating STDP to BCM. Neural Comput 15(7):1511–1523
Katz LC, Crowley JC (2002) Development of cortical circuits: lessons from ocular dominance columns. Nat Rev Neurosci 3(1):34–42
Kempter R, Gerstner W, van Hemmen JL (1999) Hebbian learning and spiking neurons. Phys Rev E 59(4):4498–4514
Kohonen T (1982) Self-organized formation of topologically correct feature maps. Biol Cybern 43(1):59–69
Kriener B, Tetzlaff T, Aertsen A, Diesmann M, Rotter S (2008) Correlations and population dynamics in cortical networks. Neural Comput 20(9):2185–2226
Leibold C, Kempter R, van Hemmen JL (2002) How spiking neurons give rise to a temporal-feature map: from synaptic plasticity to axonal selection. Phys Rev E 65(5):051915
Lubenov EV, Siapas AG (2008) Decoupling through synchrony in neuronal circuits with propagation delays. Neuron 58(1):118–131
Magee JC, Johnston D (1997) A synaptically controlled, associative signal for Hebbian plasticity in hippocampal neurons. Science 275(5297):209–213
Malsburg CV (1973) Self-organization of orientation sensitive cells in striate cortex. Kybernetik 14(2):85–100
Marinaro M, Scarpetta S, Yoshioka M (2007) Learning of oscillatory correlated patterns in a cortical network by a STDP-based learning rule. Math Biosci 207(2):322–335
Markram H, Lübke J, Frotscher M, Sakmann B (1997) Regulation of synaptic efficacy by coincidence of postsynaptic APs and EPSPs. Science 275(5297):213–215
Masquelier T, Guyonneau R, Thorpe SJ (2008) Spike timing dependent plasticity finds the start of repeating patterns in continuous spike trains. PLoS ONE 3(1):e1377
Massoulie L (1998) Stability results for a general class of interacting point processes dynamics, and applications. Stoch Proc Appl 75(1):1–30
Meffin H, Besson J, Burkitt AN, Grayden DB (2006) Learning the structure of correlated synaptic subgroups using stable and competitive spike-timing-dependent plasticity. Phys Rev E 73(4):041911
Miller KD (1996) Synaptic economics: competition and cooperation in synaptic plasticity. Neuron 17(3):371–374
Miller KD, Mackay DJC (1994) The role of constraints in Hebbian learning. Neural Comput 6(1):100–126
Moreno-Bote R, Renart A, Parga N (2008) Theory of input spike auto- and cross-correlations and their effect on the response of spiking neurons. Neural Comput 20(7):1651–1705
Morrison A, Aertsen A, Diesmann M (2007) Spike-timing-dependent plasticity in balanced random networks. Neural Comput 19(6):1437–1467
Morrison A, Diesmann M, Gerstner W (2008) Phenomenological models of synaptic plasticity based on spike timing. Biol Cybern 98(6):459–478
Neves G, Cooke SF, Bliss TVP (2008) Synaptic plasticity, memory and the hippocampus: a neural network approach to causality. Nat Rev Neurosci 9:65–75
Pfister JP, Gerstner W (2006) Triplets of spikes in a model of spike timing-dependent plasticity. J Neurosci 26(38):9673–9682
Pfister JP, Toyoizumi T, Barber D, Gerstner W (2006) Optimal spike-timing-dependent plasticity for precise action potential firing in supervised learning. Neural Comput 18(6):1318–1348
Renart A, de la Rocha J, Bartho P, Hollender L, Parga N, Reyes A, Harris KD (2010) The asynchronous state in cortical circuits. Science 327(5965):587–590
Rubin JE, Gerkin RC, Bi GQ, Chow CC (2005) Calcium time course as a signal for spike-timing-dependent plasticity. J Neurophysiol 93(5):2600–2613
Sabatini BL, Oertner TG, Svoboda K (2002) The life cycle of Ca^{2+} ions in dendritic spines. Neuron 33(3):439–452
Senn W (2002) Beyond spike timing: the role of nonlinear plasticity and unreliable synapses. Biol Cybern 87(5–6):344–355
Shadlen MN, Newsome WT (1998) The variable discharge of cortical neurons: implications for connectivity, computation, and information coding. J Neurosci 18(10):3870–3896
Sjöström PJ, Turrigiano GG, Nelson SB (2001) Rate, timing, and cooperativity jointly determine cortical synaptic plasticity. Neuron 32(6):1149–1164
Song S, Abbott LF (2001) Cortical development and remapping through spike timing-dependent plasticity. Neuron 32(2):339–350
Song S, Miller KD, Abbott LF (2000) Competitive Hebbian learning through spike-timing-dependent synaptic plasticity. Nat Neurosci 3(9):919–926
Swindale NV (1996) The development of topography in the visual cortex: a review of models. Network 7(2):161–247
Tzounopoulos T, Kim Y, Oertel D, Trussell LO (2004) Cell-specific, spike timing-dependent plasticities in the dorsal cochlear nucleus. Nat Neurosci 7(7):719–725
van Hemmen JL (2001) Theory of synaptic plasticity. In: Moss F, Gielen S (eds), Handbook of biological physics, vol 4. Neuro-

informatics and neural modelling. Elsevier, Amsterdam, pp 771–823

van Rossum MCW, Turrigiano GG (2001) Correlation based learning from spike timing dependent plasticity. Neurocomputing 38: 409–415

van Rossum MCW, Bi GQ, Turrigiano GG (2000) Stable Hebbian learning from spike timing-dependent plasticity. J Neurosci 20(23):8812–8821

Wang HX, Gerkin RC, Nauen DW, Bi GQ (2005) Coactivation and timing-dependent integration of synaptic potentiation and depression. Nat Neurosci 8(2):187–193

Wenisch OG, Noll J, van Hemmen JL (2005) Spontaneously emerging direction selectivity maps in visual cortex through STDP. Biol Cybern 93(4):239–247

Wong RO (1999) Retinal waves and visual system development. Annu Rev Neurosci 22:29–47

Zhang LI, Poo MM (2001) Electrical activity and development of neural circuits. Nat Neurosci 4:1207–1214

Zou Q, Destexhe A (2007) Kinetic models of spike-timing dependent plasticity and their functional consequences in detecting correlations. Biol Cybern 97(1):81–97